

Regionalization in global hydrological models and its impact on runoff simulations: A case study using WaterGAP3 (v 1.0.0)

Jenny Kupzig¹, Nina Kupzig², Martina Flörke¹

¹Institute of Engineering Hydrology and Water Resources Management, Ruhr-University, 44801, Bochum, Germany

²Faculty of Management and Economics, Ruhr-University, 44780, Bochum, Germany

Correspondence to: Jenny Kupzig (jenny.kupzig@rub.de)

Abstract:

Valid simulation results from global hydrological models (GHMs), such as WaterGAP3, are essential to detecting hotspots or studying patterns in climate change impacts. However, the lack of worldwide monitoring data makes it challenging to adapt GHMs' parameters to enable such valid simulations globally. Therefore, regionalization is necessary to estimate parameters in ungauged basins. This study presents the results of regionalization methods for the first time applied on the GHM WaterGAP3. It aims to provide insights into (1) selecting a suitable regionalization method for a GHM and (2) evaluating its impact on runoff simulation. In this study, four new regionalization methods have been identified as appropriate for WaterGAP3. These methods span the full spectrum of methodologies, i.e., regression-based methods, physical similarity, and spatial proximity, using traditional and machine learning-based approaches. Moreover, the methods differ in the descriptors used to achieve optimal results, although all utilize climatic and physiographic descriptors. This demonstrates (1) that different methods use descriptor sets with varying efficiency and (2) that combining climatic and physiographic descriptors is optimal for regionalizing worldwide basins. Additionally, our research indicates that regionalization leads to spatially and temporally varying uncertainty in ungauged regions. For example, regionalization highly affects southern South America, e.g., leading to high uncertainties in the flood simulation of the Río Deseado. The local impact of regionalization propagates through the water system, also affecting global estimates, as evidenced by a spread of 1,500 km³ yr⁻¹ across an ensemble of five regionalization methods in simulated global runoff to the ocean. This discrepancy is even more pronounced when using a regionalization method deemed unsuitable for WaterGAP3, resulting in a spread of 4,208 km³ yr⁻¹. This significant increase highlights the importance of carefully choosing regionalization methods. Further research is needed to enhance the predictor selection and the understanding of the methods' robustness on a global scale.

1. Introduction

Global hydrological models (GHMs) are developed and applied worldwide, e.g., to detect hotspots and examine patterns of climate change impacts on the terrestrial water cycle (e.g., Barbarossa et al., 2021; Boulange et al., 2021). Valid model results are a prerequisite to draw robust conclusions. For valid modeling results, it is beneficial to adjust the parameter values to adapt the models to different basin processes (Gupta et al., 1998). This adaptation is usually modified and evaluated (in a loop) by comparing the simulated model output, often discharge, with the monitored data. However, this parameter adjustment for GHMs is challenging due to the lack of global monitoring

37 data. Consequently, parameter adjustment for GHMs can be based not only on monitored data (i.e., calibration)
38 but also on estimating parameter values for ungauged basins (i.e., regionalization).

39 Regionalization defines the estimation of model parameters for ungauged basins (Oudin et al., 2008), usually based
40 on information from gauged basins (Oudin et al., 2010). Regionalization methods generally follow the same prin-
41 ciple: basin characteristics (e.g., physiographic and/or climatic) are linked to hydrological characteristics and can
42 thus be used to estimate parameter values. Various regionalization methods exist, and no overall preferred method
43 has been found (Ayzel et al., 2017; Pool et al., 2021). In contrast, the optimal regionalization method may differ,
44 for example, regarding available information (Pagliero et al., 2019) or model structures (Golian et al., 2021).
45 Therefore, different methods should be tested to find an optimal regionalization method for a specific use case
46 (e.g., Qi et al., 2020).

47 Evaluation is needed to assess different regionalization methods. The evaluation of regionalization methods is
48 particularly challenging because they are usually applied when there is a lack of monitoring data. Therefore, re-
49 gionalization studies often treat gauged basins as "ungauged" and perform leave-one-out cross-validation (e.g.,
50 Chaney et al., 2016) or split-sample tests (e.g., Beck et al., 2016; Nijssen et al., 2000; Yoshida et al., 2022). While
51 at the mesoscale, this evaluation is already an integral part (e.g., McIntyre et al., 2005; Parajka et al., 2005; Oudin
52 et al., 2008; Yang et al., 2020), this is sometimes not the case in global or continental studies (e.g., Müller Schmied
53 et al., 2021; Widén-Nilsson et al., 2007). Another reasonable evaluation strategy is the concept of benchmark-to-
54 beat (Schaepli & Gupta, 2007; Seibert, 2001). Applying a benchmark-to-beat supports a comprehensive evaluation
55 of whether a new approach is functional, e.g., better than a straightforward and thus transparent method or better
56 than a predecessor. To the authors' knowledge, such a benchmark-to-beat has never been used to evaluate innova-
57 tions in regionalization at a global scale.

58 In general, regionalization methods can be divided into two categories based on the parameter estimation strategy:
59 (1) regression-based and (2) distance-based (He et al., 2011). Regression-based methods derive the relationship
60 between basin characteristics and model parameters through fitted regression models. These mathematically de-
61 fined relationships are further applied to estimate model parameters of ungauged basins (e.g., Kaspar, 2004; Müller
62 Schmied et al., 2021). A significant drawback of regression-based regionalization is the difficulty of incorporating
63 parameter interdependencies (Poissant et al., 2017), as regression-based approaches often assume that the depend-
64 ent variables, i.e., the model parameters, are not correlated (Wagener et al., 2004). Distance-based approaches
65 transfer complete parameter sets from similar or nearby donor basins to ungauged basins (e.g., Beck et al., 2016;
66 Nijssen et al., 2000; Widén-Nilsson et al., 2007). Using an ensemble of donor basins, e.g., by averaging the pa-
67 rameter values or model outputs, can improve the performance of such methods (e.g., Arsenault & Brissette, 2014).
68 A significant disadvantage of such methods is the clustering problem of ungauged basins, i.e., the unequal distri-
69 bution of gauging stations worldwide (Krabbenhof et al., 2022). Thus, basins exist where distance-based ap-
70 proaches will use incomparable basins to transfer parameter values due to the lack of close basins.

71 Recent advances have implemented machine learning-based techniques in the context of regionalization. For ex-
72 ample, Chaney et al. (2016) used regression trees as an alternative to least squares regression to estimate parameter
73 values in ungauged basins. Pagliero et al. (2019) explored supervised and unsupervised clustering methods to
74 define the similarity of basins to transfer parameter sets. To the authors' knowledge, no study has compared several
75 traditional regionalization methods with machine learning-based methods for a GHM on a global scale.

76 Some regionalization methods do not make a clear distinction between calibration and regionalization. For exam-
77 ple, Arheimer et al. (2020) applied a basin grouping beforehand. Then, they jointly calibrated the group members
78 to define representative parameter sets. Subsequently, the representative parameter sets are transferred to other
79 basins based on grouping rules. Another approach defines so-called transfer functions (Samaniego et al., 2010)
80 and calibrates meta-parameters instead of the model parameter values (Beck et al., 2020; Feigl et al., 2022). These
81 methods, where regionalization is part of the calibration process, often require a change in the calibration process
82 itself, which is challenging for GHMs (Schweppe et al., 2022), for example, due to a lack of code flexibility (e.g.,
83 Cuntz et al., 2016).

84 This study proposes an improved regionalization method for the state-of-the-art GHM WaterGAP3 (Eisner, 2016).
85 It compares traditional regionalization methods with machine learning-based methods and uses a benchmark-to-
86 beat and an ensemble of split-sample tests to evaluate the applied methods. Further, global runoff simulations are
87 compared to analyze the impact of regionalization methods. The overall research topic is evaluating and selecting
88 regionalization methods for a GHM. Specifically, the study has two objectives. It aims

- 89 (1) to propose an improved regionalization method for WaterGAP3 and
- 90 (2) to evaluate the impact of regionalization methods on global runoff simulations.

91 **2. Data and Methods**

92 **2.1 The Model: WaterGAP3**

93 The GHM WaterGAP3 simulates the terrestrial water cycle, including the main water storage components and a
94 simple storage-based routing algorithm. It is a fully distributed model that operates on a five arcmin grid and
95 simulates at a daily time step. A more detailed description of the model can be found in Eisner (2016).

96 In WaterGAP3, most model parameter values are set a priori, e.g., using look-up tables for albedo or rooting depth.
97 Only one parameter, γ , is calibrated, which is part of the soil moisture storage in which runoff generation processes
98 are present. The model equation for γ , which originates from the HBV-96 model (Lindström et al., 1997), is given
99 in Eq. (1) (cf. ll. 1223-4 in `daily.cpp` of the published model (Flörke et al., 2024)). Generally, higher values of γ
100 lead to lower runoff volumes, while lower values of γ lead to higher runoff volumes. The model parameter is
101 calibrated per basin within the range of 0.1 and 5. The objective function of the calibration is to minimize the
102 deviation between the mean annual simulated and observed river discharge, i.e., the calibration aims to reduce the
103 error in discharge volume. Given the monotonic relationship between the model's parameter and the optimization
104 function, a simple search algorithm is applied: The parameter space is divided into rectangles, which are subse-
105 quently subdivided into smaller rectangles depending on the direction γ should be modified to achieve closer
106 alignment with the optimization target. The calibration results in one calibrated γ value between 0.1 and 5 per
107 basin. After the calibration, a correction is applied to account for high errors in the mass balance, e.g., due to
108 inaccuracies in global meteorological forcing products. This correction is only applicable on gauged basins. It is,
109 therefore, neglected in this study.

$$110 \quad R = P_t \cdot \left(\frac{S_s}{S_{s,max}} \right)^\gamma \quad (1)$$

111 where R is the daily runoff, P_t is the daily throughfall, S_s is the actual soil storage, $S_{s,max}$ is the maximal soil
112 storage (given as a global map in Appendix A), and γ is the calibration parameter.

113 Traditionally, the regionalization process in WaterGAP3 is a simple multiple linear regression (MLR) approach to
114 estimate the calibration parameter γ for ungauged basins (e.g., Döll et al., 2003; Kaspar, 2004). The drawback of
115 MLR regarding parameter interaction can be neglected: As there is only one parameter to estimate, parameter
116 interference does not exist. Instead, the approach offers the advantage of a lightweight, transparent application that
117 can be quickly revised and adapted.

118 2.2 Model Data

119 WaterGAP3 requires various input data, such as soil information, topography, or information on open freshwater
120 bodies. This study uses the same input data as Kupzig et al. (2023). For meteorological forcing, we use the global
121 data set EWEMBI (Lange, 2019). This data product includes daily global forcing data with a spatial resolution of
122 0.5 degrees (latitude and longitude) that covers a period from 1979 to 2016. Specifically, WaterGAP3 uses the
123 following forcing information from the EWEMBI data set as input:

- 124 • daily mean temperature,
- 125 • daily precipitation,
- 126 • daily shortwave downward radiation, and
- 127 • daily longwave downward radiation.

128 The WaterGAP3 calibration requires observed monthly river discharge data. This discharge data is subsequently
129 transformed into annual discharge sums and used as a benchmark in the calibration procedure. In this study, we
130 used discharge data from 1,861 stations that were manually verified (Eisner, 2016). To get the best data available,
131 we have updated all available station data with recent data from The Global Runoff Data Center (GRDC, 2020).
132 All stations have at least five years of complete (monthly) station data between 1979 and 2016. For each station,
133 a contribution area, i.e., a basin, is defined with the gridded flow-direction information obtained from WaterGAP3,
134 based on the HydroSHEDS database (Lehner et al., 2008).

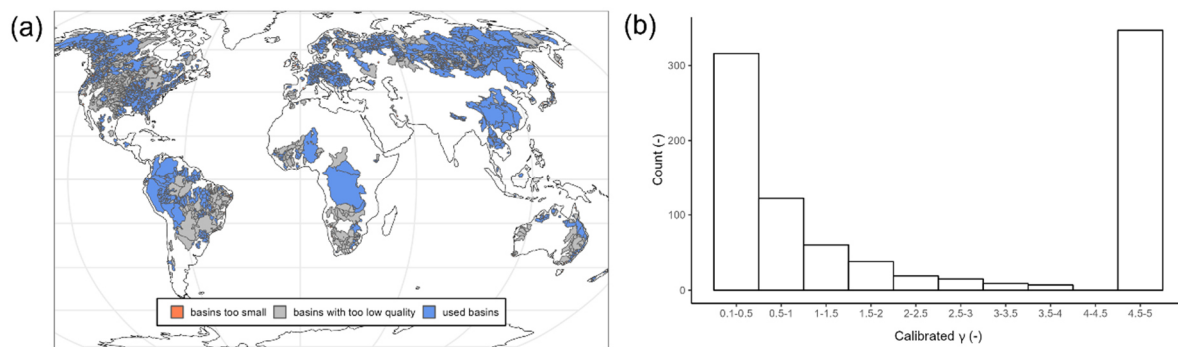
135 The 1,861 basins are calibrated using the above-described standard calibration approach for WaterGAP3. Follow-
136 ing the standard calibration procedure, some basins still have an insufficient model performance. In this context,
137 we define a monthly Kling-Gupta-Efficiency (KGE) (Gupta et al., 2009) below 0.4 or more than 20 % bias in
138 monthly flow as insufficient model performance. The expression for the KGE is given in Eq. (2). We underscore
139 the importance of minimizing the error in discharge volume by defining it as an additional criterion corresponding
140 to the optimization target during calibration. Basins not fulfilling the defined conditions regarding bias and KGE
141 are neglected in further analysis to avoid high parameter uncertainty due to errors in input data, model structure,
142 or discharge data affecting the analysis. Further, we have excluded all basins with less than 5000 km² (inter-) basin
143 size from the next upstream basin. We assume that this inter-basin size is large enough to assume a certain degree
144 of interdependency between nested basins. In total, 933 out of 1,861 basins are selected for regionalization (626
145 are neglected due to insufficient model performance, and 302 are neglected due to inadequate basin size).

$$146 \quad KGE = 1 - \sqrt{(1 - r)^2 + \left(1 - \frac{\sigma_y}{\sigma_x}\right)^2 + \left(1 - \frac{\mu_y}{\mu_x}\right)^2} \quad (2)$$

147 where r is the Pearson correlation coefficient between observed discharge x and simulated discharge y , σ denotes
148 the corresponding standard deviation, and μ the corresponding mean of observed and simulated discharge.

149 Figure 1a depicts the worldwide calibrated basins, highlighting gauged and ungauged regions. Whereas most parts
150 of North and South America are gauged, Africa and Australia remain largely ungauged. A cluster of gauged basins
151 is in Central Europe and in Eastern Asia. Gauged regions with insufficient model performance are mainly in the
152 Mississippi River basin, Southern Africa, Australia, and large parts of Brazil. These regions are known to be chal-
153 lenging for GHMs (e.g., cf. Fig. 8b in Stacke & Hagemann, 2021).

154 Figure 1b shows the calibrated values for γ . It emerges that the calibrated values tend to be at the upper and lower
155 bounds of the parameter space. This behavior is already known (cf. Fig. 4b in Müller Schmied et al., 2021). A
156 brief sensitivity analysis and discussion of the calibration parameter are included in Appendix B. The results of
157 this analysis indicate that the clustering of the calibrated parameter value is not related to an inappropriate selection
158 of the parameter bounds but instead to the absence or an insufficient representation of processes. Thus, the clus-
159 tering of the calibrated values does not indicate an inadequate selection of the parameter bounds but highlights the
160 necessity to improve the model structure and the calibration strategy for WaterGAP3. However, this study focuses
161 solely on analyzing and implementing regionalization methods. It does not aim to enhance the model structure or
162 to change the calibration procedure of WaterGAP3. Future studies are needed to achieve the latter, as WaterGAP3
163 contains many hard-coded parameters or parameters defined by look-up tables that need to be analyzed to identify
164 and adjust sensitive parameters more accurately during calibration. Initial steps in this direction have already been
165 taken for WaterGAP2 in the form of a multivariate and multi-objective case study in the Mississippi River basin
166 (Döll et al., 2024).



167
168 **Figure 1: a) Map of calibrated basins, highlighting basins not used for regionalization due to insufficient model perfor-**
169 **mance or inadequate basin size and b) the histogram of the calibrated γ values for all used basins showing a cluster of**
170 **parameter values at the parameter bounds.**

171 2.3 Basin Descriptors

172 This study uses basin descriptors as predictors to drive regression-based or distance-based regionalization ap-
173 proaches. These basin descriptors are based on data used within the model simulation (as they are globally avail-
174 able). They are aggregated to basin values using a simple mean method to have the same spatial resolution as the
175 calibrated model parameter. Thus, in the case of nested basins, the inter-basin area is used to define the basin
176 descriptors. The selection of the predictors, i.e., basin descriptors that support the estimation of γ , is crucial for
177 regionalization methods (Arsenault & Brissette, 2014). Typically, this selection aims to obtain the most infor-
178 mation with the least number of predictors to (1) improve the model quality and (2) limit over-parametrization. In
179 this study, we use 12 basin descriptors to develop regionalization methods; nine of these descriptors are physio-
180 graphic, while the remaining three are climatic (see Table 1). Most descriptors are not correlated (see Appendix
181 C), i.e., we minimize redundant information (Wagener et al., 2004).

182 A descriptor subset is selected based on correlation analysis between basin descriptors and calibrated γ value and
183 entropy assessment. Pearson's correlation coefficient detects linear correlation, and Spearman's Rho and Kendall's
184 Tau detect a non-linear correlation. Shannon entropy (Shannon, 1948) measures the information gain of the pre-
185 dictors explaining the calibrated γ value. The higher the information gain, the more valuable the basin descriptor
186 is for explaining the variation in the calibrated γ value. The analysis directly evaluates the relationship between
187 the calibrated parameter and the basin descriptors, as WaterGAP3 uses only one calibration parameter with a clear
188 global optimum within the parameter space. An alternative would be to use flow characteristics to define the basis
189 for regionalization (e.g., Pagliero et al., 2019). We decided to use the calibrated parameter instead of flow charac-
190 teristics as it does not need any further assumption on which flow characteristics determine the model's parameter.

191 Statistical information of the evaluated basin descriptors and the corresponding correlation coefficients and infor-
192 mation gain are listed in Table 1. The basin descriptors demonstrate a considerable degree of variability, e.g., the
193 basin size ranges from 5000 km² to 3,112,480 km² with a median of 13,796 km². The mean temperature varies
194 from -19 °C to 29 °C, and the sum of precipitation ranges from 213 mm to 5,716 mm. Although there is a high
195 degree of variability in the analyzed basin descriptors, the basin descriptors exhibit low correlation coefficients
196 with the calibrated values. For example, the permafrost coverage shows the strongest Pearson correlation of -0.37
197 (and -0.50 for Spearman's Rho). The information gain indicates the same results as the correlation analysis, i.e.,
198 the information gain is generally relatively low, and descriptors with a higher correlation tend to have a higher
199 information gain. For example, the mean temperature exhibits the maximal information gain of 17.6 % and has
200 the second-highest correlation coefficient with a Pearson correlation of 0.34.

201 **Table 1: Basin descriptors: statistical information, correlation, and entropy assessment. Selected physiographic and**
202 **climatic basin descriptors are written in bold.**

	Basin Descriptor	Attribute Information				Entropy & Correlation			
		Min	Max	Mean	Median	IG (%) ¹	Pearson	Spearman	Kendall
physiographic	Soil Storage (mm)	12.405	610.469	220.805	195.778	13.07	-0.21	-0.15	-0.11
	Open Water Bodies (%)	0.000	63.960	5.521	1.812	5.65	-0.01	-0.08	-0.05
	Wetlands (%)	0.000	63.466	4.164	0.547	5.01	-0.02	-0.13	-0.09
	Size (km ²)	5000	3,112,480	37,572	13,796	1.42	-0.04	-0.04	-0.03
	Slope Class (-)	10.057	67.756	38.668	38.364	16.60	-0.31	-0.37	-0.27
	Altitude (m.a.s.l.)	30.239	4765.166	591.024	394.870	9.30	-0.18	-0.28	-0.20
	Sealed Area (%)	0.000	12.3	0.6	0.1	4.49	0.22	0.38	0.29
	Forest (%)	0.000	100.000	35.340	24.002	13.82	-0.25	-0.18	-0.14
	Permafrost & Glacier (%)	0.000	95.000	16.662	0.000	13.12	-0.37	-0.50	-0.40
climate	Mean Temperature(°C)	-18.848	28.823	7.720	7.707	17.56	0.34	0.41	0.30
	Yearly Precipitation (mm)	213.6	5,716.3	996.5	779.5	9.23	0.02	0.21	0.14
	Yearly Shortwave Down-ward Radiation (Wm⁻²)	1,050.6	3,043.2	1,857.9	1,759.7	15.79	0.31	0.33	0.24

¹Information gain is given in percentage of total information content in γ after Shannon (1948)

203 In contrast to the findings of Wagener and Wheeler (2006), the correlation coefficients between the basin de-
204 scriptors and the calibrated values are relatively low, indicating a weak relationship. One potential explanation for
205 this discrepancy is that Wagener and Wheeler (2006) used a smaller number of basins in southeast England, with
206 limited versatility (e.g., regarding climate and seasonality) compared to the 933 worldwide basins used in this
207 study. Studies using a large number of basins likely tend to find a lower correlation between catchment attributes

208 and model parameters (Merz et al., 2004). Moreover, the clustered calibrated γ values at the bounds of the valid
209 parameter space may disturb the results of this analysis. As the calibrated value masks the effect of multiple sources
210 of errors, such as uncertainty in the input data, model structure, or varying hydrological processes, finding a mean-
211 ingful relationship between catchment characteristics and calibrated values is challenging.

212 Because the basis for the descriptor selection seems uncertain, given the low correlation and the named constraints,
213 we additionally run the regionalization methods with all descriptors to evaluate the descriptor selection. Further
214 on, to ascertain the advantage of integrating climatic descriptors, we run the regionalization methods using either
215 physiographic or climatic descriptors. In total, we used four groups of basin descriptors to implement the region-
216 alization methods:

- 217 • "cl": all three climatic descriptors,
- 218 • "p": all nine physiographic descriptors,
- 219 • "p+cl": all 12 descriptors, and
- 220 • "subset": two correlated climatic descriptors (mean temperature, annual shortwave radiation) & three
221 correlated physiographic descriptors (slope class, forest %, permafrost %).

222 2.4 Regionalization Methods

223 In our study, we test several traditional and machine learning-based regionalization methods against each other
224 and a defined benchmark-to-beat to find suitable regionalization methods for WaterGAP3. At the global scale,
225 regionalization is particularly challenging due to (1) the lack of high-quality data, (2) the diversity of dominant
226 hydrological processes in basins, and (3) the high computational demands of the models. Therefore, a robust re-
227 gionalization method that applies to a wide variety of basins and is not computationally demanding should be
228 selected for a global application.

229 We test three common traditional approaches and two machine learning-based approaches using the concepts of
230 spatial proximity, physical similarity, and regression-based methods. As WaterGAP3's model calibration is very
231 rigid and has only one parameter, it is not feasible to implement and test regionalization methods that incorporate
232 regionalization into the calibration process, such as transfer functions. In addition, we avoid high computational
233 demands as all evaluated methods are applicable after the calibration, i.e., without running the model.

234 As the calibration of WaterGAP3 results in a parameter distribution with a cluster of parameter values at the
235 parameter bounds, we implement a so-called "tuning" to introduce information about the parameter space into
236 regionalization. In detail, we apply a simple threshold-based approach to shift the regionalized parameter values
237 to the extremes, i.e., $\gamma_{est} < \gamma_1 \rightarrow \gamma_{reg} = 0.1$ and $\gamma_{est} > \gamma_2 \rightarrow \gamma_{reg} = 5.0$. The thresholds γ_1 and γ_2 are defined
238 by applying the k-means algorithm with three centers to the calibrated parameter values. This clustering results in
239 three clusters: one for low, one for medium, and one for high γ values. Subsequently, γ_1 refers to the highest γ
240 value of the low cluster and γ_2 refers to the lowest γ value of a high cluster.

241 To evaluate the regionalization methods, we implement an ensemble of split-sample tests. Specifically, we ran-
242 domly split the basins into 50 % gauged (for training) and 50 % pseudo-ungauged (for testing). The split has a
243 relatively high percentage of pseudo-ungauged basins, accounting for many missing gauges worldwide and the
244 high importance of generalizability. We fit the methods and apply them to the training and testing data sets. The
245 split-sample test is repeated 100 times by randomly splitting the basins to account for sampling effects.

246 As there is only one calibration parameter, γ , this parameter has a global optimum per basin. Consequently, the
 247 quality of training and testing is directly assessed by the deviation between the regionalized and the calibrated
 248 value for γ . The closer the regionalized values are to the calibrated ones, the more accurate the prediction. We
 249 assess the prediction accuracy by the logarithmic version of the mean absolute error (logMAE) shown in Eq. (3)
 250 to account for the decreasing sensitivity of γ for higher values (see Appendix B). The lower the logMAE, the better
 251 the prediction; a zero value in logMAE expresses no error. The regionalization method is robust if the prediction
 252 accuracy is similar in training and testing. A generally good performance, i.e., small logMAE values, indicates
 253 that the regionalization method suits WaterGAP3. The comparison of γ values enables applying a wide range of
 254 regionalization methods and sets of descriptors, as no computationally intensive model simulation is required.
 255 However, it assumes that deviations in γ lead, in turn, to deviations in discharge, which is only partially true
 256 because of varying parameter sensitivity in basins (e.g., Kupzig et al., 2023). To validate that the logMAE is a
 257 sufficient approximator for the regionalization performance in WaterGAP3, we use one representative split-sample
 258 from the ensemble to compare the accuracies in simulated discharge for different regionalization methods.

$$259 \logMAE = \frac{1}{n} \sum |\ln(\gamma_{x,i} + 1) - \ln(\gamma_{y,i} + 1)| \quad (3)$$

260 where n is the number of basins in the corresponding sample, $\gamma_{x,i}$ is the calibrated value of γ for the i^{th} basin, and
 261 $\gamma_{y,i}$ is the estimated value of γ for the i^{th} basin. We applied a Box-Cox-type transformation with $\lambda_1=0$ and $\lambda_2=1$
 262 (Box and Cox, 1964) to calculate the logMAE, avoiding negatively transformed values.

263 **Regression-based methods**

264 The traditionally used regionalization approach of WaterGAP3 is a regression-based MLR. As the benchmark-to-
 265 beat, we use the regionalization approach from WaterGAP2.2d defined in Müller Schmied et al. (2021). We con-
 266 sider it a suitable benchmark-to-beat given that WaterGAP2 has a model structure and calibration process that is
 267 very similar to WaterGAP3. The main difference between these models is that WaterGAP2 simulates at 0.5° spatial
 268 resolution. The benchmark-to-beat consists of "a multiple linear regression approach that relates the natural loga-
 269 rithm of γ to basin descriptors (mean annual temperature, mean available soil water capacity, fraction of local and
 270 global lakes and wetlands, mean basin land surface slope, fraction of permanent snow and ice, aquifer-related
 271 groundwater recharge factor)". (Müller Schmied et al., 2021) We fit this regression model to our data and define
 272 the quality of this approach as the benchmark-to-beat. Moreover, we test an independent MLR approach without
 273 using the logarithmic scaling of γ and using the above-defined sets of basin descriptors. For MLR and the bench-
 274 mark-to-beat, we use the `lm()` function of the R package `stats` (R Core Team, 2020). After applying the regression
 275 model, we adjust the estimated parameter values to ensure that the estimated values range between 0.1 and 5.

276 Furthermore, a machine learning-based method, random forest (RF), is tested for regionalization as an alternative
 277 to MLR. Here, we implement the random forest algorithm with the `randomForest()` function from the R package
 278 `randomForest` (Liam & Wiener, 2002), which is based on Breiman (2001). The algorithm uses an ensemble of
 279 decision trees, making the decision human-like. It is relatively robust because it incorporates random effects into
 280 the training process. To implement this randomness, we define the algorithm as one that can choose between two
 281 randomly selected predictors at each node, using an ensemble of 200 trees.

282 **Physical Similarity**

283 As the traditional physical similarity approach, we use Similarity Indices (in the following named with SI), apply-
284 ing the methodology proposed by Beck et al. (2016). The SI (see Eq. (4)) are derived using the defined basin
285 descriptors sets, and the parameter of the most similar basin is transferred to the pseudo-ungauged basin. Addi-
286 tionally, we use an ensemble of basins to control whether an ensemble-based approach leads to more robust results.
287 The optimal number of donor basins may vary between research regions and hydrological models (Guo et al.,
288 2020). Here, we use ten donor catchments (noted with "ensemble") based on Beck et al. (2016) and McIntyre et
289 al. (2005). Further, we apply a simple mean method for the ensemble-based prediction to aggregate the ensemble
290 of γ values into one predicted parameter value.

$$291 \quad S_{i,j} = \sum_{p=1}^n \frac{|Z_{p,i} - Z_{p,j}|}{IQR_p} \quad (4)$$

292 where $S_{i,j}$ is the Similarity Index between basin i and basin j , $Z_{p,j}$ is the basin descriptor p for basin j , IQR_p is the
293 interquartile range for basin descriptor p among all (gauged) basins, and n is the number of all basin descriptors
294 used.

295 As an alternative machine learning-based approach, we apply a simple k-means algorithm. We selected the k-
296 means algorithm because it is one of the most widely used clustering algorithms (Tongal & Sivakumar, 2017). It
297 is easy to understand and use. The algorithm `kmeans()` is implemented in the R base package `stats`. It aims to
298 maximize variation between groups and minimize variation within groups. The number of clusters to use is deter-
299 mined by multiple indices calculated with the R package `NbClust` (Charrad et al., 2014). For all 933 basins and
300 the defined sets of basin descriptors, most indices defined three as the optimal number of clusters. Accordingly,
301 we use three clusters to generate the groups of basins. As different scales of the predictor values can affect the
302 clustering, a rescaling with min-max-normalization (see Eq. (5)) is performed on the training set and applied to
303 the testing set. After the grouping, the mean γ value is assigned as a representative calibrated value to the corre-
304 sponding basin group. To estimate the corresponding group for a pseudo-ungauged basin, the `knn` algorithm is
305 used, and the representative γ value of the group is assigned to the pseudo-ungauged basin. This algorithm is
306 implemented by the `knn()` function of the R package `class` (Venables & Ripley, 2002). Since the k-means method
307 is less flexible than SI, we implement a highly flexible version, using the `knn` algorithm directly to define the donor
308 basin most similar to each ungauged basin. Using the `knn` algorithm directly, we test how beneficial it is to create
309 groups of similar basins using the `kmeans` algorithm and regionalize the parameter with a representative mean
310 value.

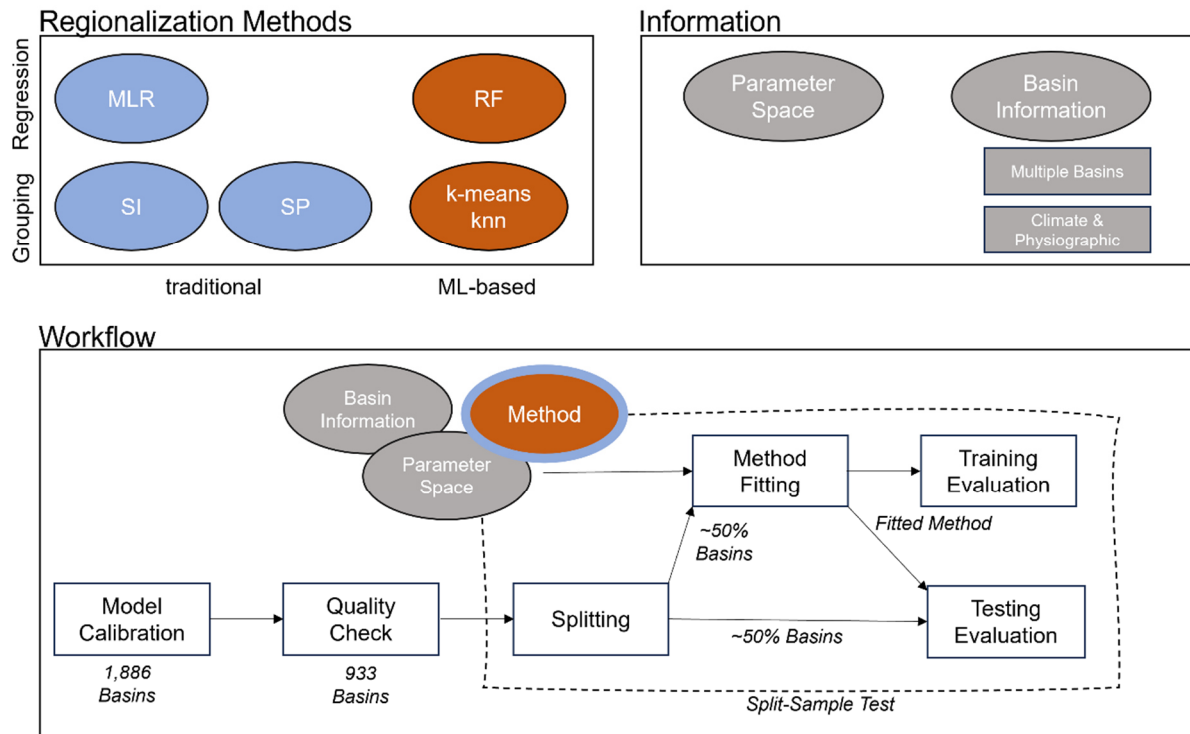
$$311 \quad Z'_{p,j} = \frac{Z_{p,j} - \min_{j \rightarrow m}(Z_{p,j})}{\max_{j \rightarrow m}(Z_{p,j}) - \min_{j \rightarrow m}(Z_{p,j})} \quad (5)$$

312 where $Z'_{p,j}$ is the normalized basin descriptor p for basin j , $Z_{p,j}$ is the basin descriptor p for the basin j , m is the
313 number of (gauged) basins.

314 **Spatial Proximity**

315 The spatial proximity approach is one of the easiest to regionalize parameter values. However, it is also often
316 criticized that nearby basins do not necessarily have the same hydrological behavior (Wagener et al., 2004). Fur-
317 thermore, its performance depends on the density of the network of gauged basins (Lebecherel et al., 2016). The

318 dependency on network density is particularly challenging for global applications where large parts of the world
 319 are ungauged (e.g., northern Africa). Nevertheless, the approach has been successfully applied in other studies
 320 (e.g., Oudin et al., 2008; Qi et al., 2020), even globally (Widén-Nilsson et al., 2007). Here, we take the distance
 321 between the centroids of the basins as the reference for the spatial distance between basins, as done by others
 322 (Oudin et al., 2008; Merz and Blöschl, 2004). We use the abbreviation SP in the text below to refer to the spatial
 323 proximity approach. Figure 2 provides an overview of the applied regionalization methods and information used
 324 for the experimental setup.



325
 326 **Figure 2: Experimental setup of the study: regionalization methods, used modifications and information, and the gen-**
 327 **eral workflow (MLR: Multiple Linear Regression, SI: Similarity Indices, SP: Spatial Proximity, RF: RandomForest).**

328 3. Results and Discussion

329 3.1 Evaluating the effect of tuning

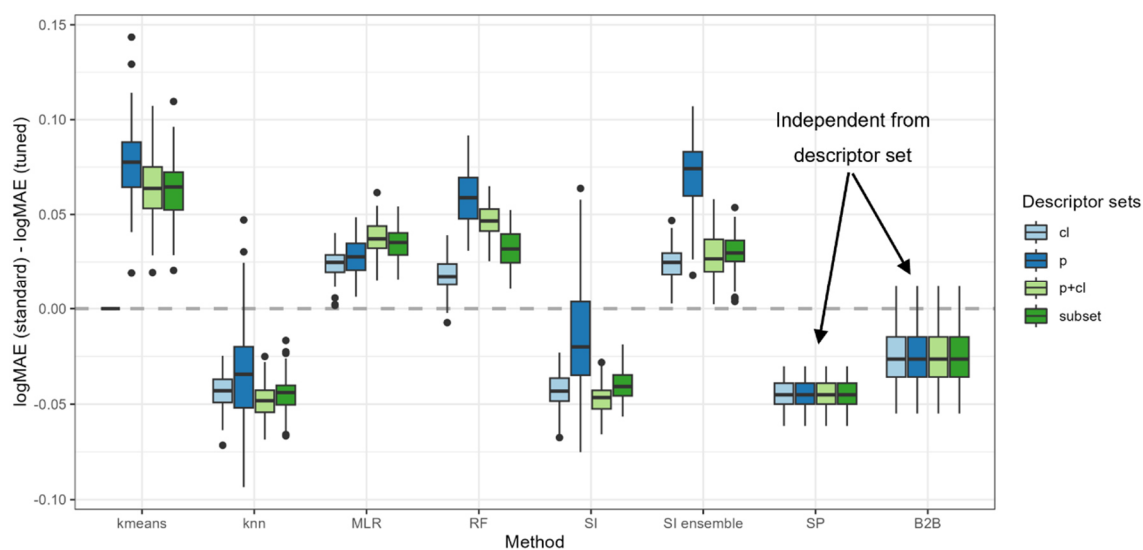
330 First, the impact of the tuning approach on the regionalization approaches is evaluated. Therefore, Fig. 3 depicts
 331 the differences in logMAE between the standard and tuned approaches in testing, i.e., using the pseudo-ungauged
 332 basins. A positive difference in logMAE indicates an increase in accuracy, whereas a negative difference indicates
 333 a decrease in accuracy due to the tuning.

334 Using the tuning thresholds of about 1.1 and 3.4 for γ_1 and γ_2 , respectively, enhances the predictive accuracy for
 335 kmeans, MLR, RF, and the ensemble approach of SI. The most remarkable improvement for kmeans, RF, and SI
 336 ensemble is achieved when all physiographic descriptors are used as input (mean improvement of 0.077, 0.058,
 337 and 0.071, respectively). MLR shows the most significant improvement when using all available descriptors (mean
 338 improvement of 0.038). In contrast, the tuning decreases the performance for knn, SI, and SP, with a mean degra-
 339 dation between -0.02 and -0.05. Unlike the enhanced regionalization techniques, these methods transfer single-
 340 basin information to ungauged regions. Thus, the tuning disturbs the use of single-basin information yet simulta-

341 neously enhances the performance of methods that transfer multi-basin information. The disturbance or improve-
 342 ment is probably related to the capability of the methods representing the clustering of parameter values at the
 343 extremes: Whereas the multi-basin information transfer implies a smoothing and thus suffers from a lack of rep-
 344 resenting the extremes, the single-basin information transfer exhibits no such a smoothing.

345 The exception from the above-defined rule is the benchmark-to-beat approach. The benchmark-to-beat is the only
 346 approach that uses logarithmic scaled γ values when fitting the model. This logarithmic transformation leads to an
 347 increase in estimating small values. Thus, when the benchmark-to-beat is tuned, more basins with higher calibrated
 348 γ values receive low estimates. The tuning intensifies this effect, leading to a decrease in the accuracy of the
 349 logMAE from the standard to the tuned version. Thus, for models using logarithmical transformed γ values, the
 350 defined thresholds for the tuning are not appropriate.

351 Applying knowledge of the optimal parameter space enhances the quality of regionalization for methods transfer-
 352 ring multi-basin information in case the tuning thresholds are appropriate. This positive effect is not surprising, as
 353 incorporating a priori information about parameter distribution strengthens parameter estimation (e.g., described
 354 in Tang et al. (2016) using the Bayes Theorem). However, for single-basin transfer, which already represents the
 355 parameter space well, i.e., the clustering of γ at the extremes, the tuning disturbs the performance. This indicates
 356 that such tuning needs to be cautiously introduced as there is the risk of decreasing the accuracy of regionalization.



357
 358 **Figure 3: Changes in performance between standard and tuned versions for all applied regionalization approaches.**
 359 **Positive values indicate an improvement related to the tuning.**

360 3.2 Evaluating descriptor subsets & algorithm selection

361 Different descriptor sets yield different performances in regionalizing γ . Table 2 shows the median of all logMAE
 362 values for the testing. For a complete overview of the results of the split-sample test ensemble, see Appendix D.
 363 Evaluating Table 2 reveals that the selected subset or all descriptors consistently yield the best performance across
 364 all regionalization methods. In both variants of the ensemble approach of SI, the tuned version of the no-ensemble
 365 approach of SI, and the standard version of RF, the selected subset yields the best results. For all other methods,
 366 using all descriptors yields the best results. Hence, all methods perform best when combining climatic and physi-
 367 ographic descriptors. This benefit of using climatic and physiographic descriptors is consistent with others that
 368 often apply a combination of climatic and physiographic descriptors, achieving optimal regionalization results
 369 (e.g., Oudin et al., 2008; Reichl et al., 2009).

370 The machine learning-based approaches seem to benefit most when using more information displaying an im-
 371 mprovement for all methods (knn, kmeans, and RF) and both variants (standard and tuned) ranging from "cl", "p",
 372 "subset" to "p+cl". This is not surprising as machine learning is developed to deal with big data sets. The traditional
 373 methods MLR and SI do not exhibit such a distinct pattern. The (weakly) correlated subset of climatic and physi-
 374 ographic descriptors yields the best results for SI. As utilizing all descriptors decreases the performance slightly,
 375 the results indicate that uncorrelated descriptors may disturb the performance of this approach. For MLR, the
 376 meaning of physiographic information is highest, resulting in the best ("p+cl") and second best ("p") results. The
 377 disparate performance of the regionalization methods when using different descriptor sets indicates that different
 378 methods use descriptor sets with varying efficiency. It also emphasizes that the selection of descriptors impacts
 379 the regionalization method's results, as noted by others (Arsenault & Brissette, 2014). Consequently, the above-
 380 performed analysis defining a descriptor subset lacks universal validity as methods exist where the defined subset
 381 is outperformed. Instead, the validity of this approach is most closely aligned with the SI approaches.

382 Although the algorithms kmeans and knn are similar, they yield considerably different performances in Table 2.
 383 As knn shows a logMAE of 0.432 at best, the kmeans algorithm performs poorly, resulting in the best logMAE of
 384 0.472. This indicates that applying the kmeans clustering algorithm to transfer averaged parameters is inappropri-
 385 ate for WaterGAP3. This may be attributed to the reduced flexibility of the approach, which entails estimating
 386 only three γ values due to the optimal, though limited, number of centers. The ensemble SI approach consistently
 387 outperforms the no-ensemble SI approach in almost all variants. The positive effect of an ensemble approach for
 388 SI has already been noted (Oudin et al., 2008). Therefore, it is recommended that the number of donor basins
 389 derived from the literature be adopted in future applications to be optimal for WaterGAP3, likely resulting in
 390 higher performance.

391 **Table 2: Median logMAE of 100 split-samples for pseudo-ungauged basins, i.e., in testing, for all regionalization meth-**
 392 **ods applying four sets of descriptors for a) the standard version and b) the tuned version. The bold numbers indicate a**
 393 **better performance than the benchmark-to-beat. Thicker edges mark best-performing variants, which are chosen for**
 394 **further analysis. Grey-shaded cells indicate worst-performing variants, which were taken to validate the assumption**
 395 **that lower logMAE values result in lower KGE values.**

(a)

test (median)	MLR	RF	SI		kmeans	knn	SP	B2B
			no ens.	ensemble				
cl	0.552	0.483	0.496	0.483	0.619	0.501	0.454	0.461
p	0.479	0.465	0.487	0.480	0.551	0.477		
p+cl	0.464	0.464	0.454	0.462	0.534	0.432		
subset	0.488	0.488	0.461	0.439	0.539	0.467		

(b)

test* (median)	MLR	RF	SI		kmeans	knn	SP	B2B
			no ens.	ensemble				
cl	0.529	0.467	0.537	0.459	0.619	0.546	0.502	0.488
p	0.441	0.416	0.532	0.455	0.515	0.521		
p+cl	0.427	0.403	0.503	0.435	0.472	0.480		
subset	0.453	0.408	0.501	0.409	0.477	0.509		

396 Only a few regionalization methods outperform the benchmark-to-beat. The best descriptor sets of tuned MLR,
 397 RF, and SI ensemble approach have a logMAE of 0.427, 0.403, and 0.409, respectively. The standard version of

398 knn ("p+cl") and SP yield 0.432 and 0.454 in logMAE, respectively. Additionally, two variants of the standard SI
399 approaches outperform the benchmark-to-beat yet exhibit inferior results compared to the selected tuned approach.
400 All other regionalization methods show higher logMAE values than the benchmark-to-beat. These methods are
401 considered insufficient in terms of performance to regionalize γ in WaterGAP3. As the benchmark-to-beat outper-
402 forms all kmeans approach variants, it is deemed unsuitable for regionalizing γ for WaterGAP3 and, therefore,
403 excluded from further analysis.

404 The well-performing SP on a global scale is surprising as the distances between basins are potentially long, and
405 hydrological processes may strongly vary. It is probably beneficial for the SP approach that γ comprises all kinds
406 of errors, e.g., spatially localized errors in global forcing products (e.g., Beck et al., 2017 reported errors for arid
407 regions in the precipitation product) or inaccurately represented processes for larger regions. Thus, the estimation
408 of γ might be appropriate, but not because of the same hydrological behavior but due to the same kind of errors.

409 The RF approach is outstanding, as it shows a massive loss in performance from training to testing (see Appendix
410 D). In detail, the logMAE in testing is about twice the logMAE in training. In comparison, other methods show
411 values of logMAE in testing ranging from 95.6 % to 101.4 % of logMAE in training. This performance loss indi-
412 cates that RF is not a robust regionalization method for WaterGAP3. Other studies that reported the good perfor-
413 mance of RF for regionalization have not investigated the stability of the performance from training to testing
414 (Golian et al., 2021; Wu et al., 2023). Likely, the mathematical problem of predicting the calibrated parameter for
415 WaterGAP3, with all its challenges (e.g., tailored parameter space, clustered calibrated parameter, and incorpora-
416 tion of many sources of errors), cannot be adequately solved by RF. Thus, although RF is known to be especially
417 robust among other machine learning-based techniques, it shows symptoms of over-parameterization. This indi-
418 cates that the algorithm is too flexible and adjusts to noise in the data, missing the underlying systematic. This lack
419 of robustness is particularly disadvantageous since, for WaterGAP3, regionalization is applied globally, requiring
420 regionalizing large parts of the world. In consequence, the RF approach is left out from further analysis and defined
421 as not suitable to regionalize γ for WaterGAP3.

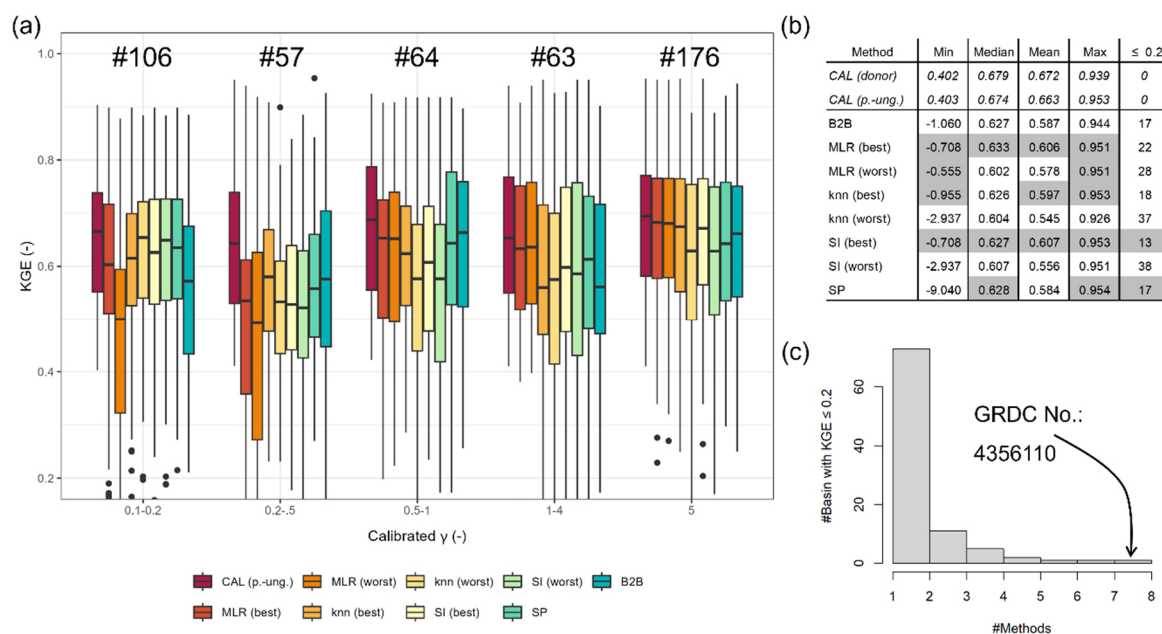
422 For the tuned MLR approach and the knn approach, the best performing and, therefore, selected variant employs
423 all 12 descriptors. This number of predictors for a regionalization method is among the highest found in the liter-
424 ature (e.g., McIntyre et al., 2013, used three predictors; Beck et al., 2016, used eight predictors; Chaney et al.,
425 2010, used 13 predictors). In general, it is advisable to limit the number of degrees of freedom in a model to reduce
426 the risk of over-parametrization, thus increasing the probability of generalizability (Seibert et al., 2019). As both
427 model variants exhibit a stable model performance during training and testing (see Table D1), using a high pro-
428 portion of the basins for testing, i.e., 50 %, we consider the two variants robust despite the relatively high number
429 of predictors used. Therefore, we consider them appropriate for further model evaluation.

430 Nevertheless, the chosen basin descriptors for knn and tuned MLR could be enhanced in future studies. As the
431 descriptor set "p+cl" was initially considered as a control group to determine the suitability of the selected subset,
432 it is not optimal. To indicate potential enhancements regarding the descriptor set for both methods, we calculated
433 a simple permutation-based feature importance score (cf. Breiman, 2001) by randomly shuffling each predictor
434 within the testing data set and quantifying the loss in logMAE relative to the logMAE of the original testing data
435 set. The higher the loss, the more critical the shuffled predictor for the regionalization method. The resulting feature

436 importance scores are presented in Appendix E, indicating that for the tuned MLR, the subset of (weakly) corre-
 437 lated descriptors should be extended by including waterbody information. For the knn approach, the calculated
 438 feature importance scores indicate that it should be extended by including information about the soil storage.

439 3.3 Performance of selected algorithm in pseudo-ungauged basins

440 To avoid the high risk of sampling effect when applying the split-sample test, we conduct an ensemble of 100
 441 split-sample tests analyzing the median of logMAE between regionalized and calibrated values as an indicator for
 442 performance. Directly using the differences in regionalized and calibrated values is only meaningful when the
 443 calibrated value represents the global optimum. As this is often not the case, e.g., due to equifinality, the perfor-
 444 mance of regionalization methods is usually assessed by the accuracy of simulated discharge (e.g., Samaniego et
 445 al., 2010; Arsenault & Brissette, 2014). Because WaterGAP3 requires computationally intensive simulations, run-
 446 ning WaterGAP3 for all 100 split-sample tests for the selected methods is not feasible. Therefore, we select a
 447 single representative split-sample to assess the quality of representing the discharge in the pseudo-ungauged basins
 448 using regionalized γ values. The representative split-sample leads to comparable logMAE values to the corre-
 449 sponding median of the ensemble for all regionalization methods. For the evaluation, WaterGAP3 was run for the
 450 same period used in calibration (from 1979 to 2016), with the first year simulated ten times to allow for model
 451 warm-up. Using this period ensures the availability of sufficient data for the evaluation (see Chapter 2.2). Further-
 452 more, the differences between the monthly simulated and observed discharge are assessed using the KGE.



453
 454 **Figure 4: a) KGE values of pseudo-ungauged basins from split-sample test grouped by the range of calibrated γ values,**
 455 **b) selected metrics of KGE values from the pseudo-ungauged basins (better or equal performance to the benchmark-**
 456 **to-beat is highlighted in grey), and c) histogram of the number of pseudo-ungauged basins with a KGE below 0.2 and**
 457 **the corresponding number of methods exhibiting this performance loss.**

458 To evaluate the KGE, we select the best-performing methods that outperform the benchmark-to-beat: tuned MLR
 459 "p+cl", knn "p+cl", tuned SI ensemble "subset", and SP (see Table 2). For the sake of simplicity, we further mark
 460 them with "(best)". Additionally, we select three poorly performing variants to validate the assumption that meth-
 461 ods resulting in higher logMAE values tend to result in lower KGE values, i.e., lower accuracy of simulated dis-

462 charge. These methods are tuned SI "cl" (logMAE: 0.537), tuned knn "cl" (logMAE: 0.546), and MLR "cl" (log-
463 MAE: 0.552). Further, we denote these methods with "worst". Applying the selected methods and the benchmark-
464 to-beat method results in eight estimates of γ for the pseudo-ungauged basins, whose performance is further eval-
465 uated in terms of simulated discharge accuracy.

466 Figure 4a shows the resulting KGE values for the evaluated regionalization methods and the calibrated version as
467 grouped boxplots for different ranges of calibrated γ . The methods show different performances for different γ
468 ranges, indicating their strengths and weaknesses. For the smallest γ range, "0.1-0.2", the selected methods that
469 perform well during the split-sample test outperform the benchmark-to-beat. The better result for minimal γ ranges
470 is probably partially related to the advantage of the tuning, which leads to more predictions of 0.1 within the
471 regionalization. The benchmark-to-beat shows the best performance for γ values between 0.2 and 0.5. The good
472 performance for basins with calibrated γ values between 0.2 and 0.5 is probably related to the benefit of using the
473 logarithmical version of γ in the benchmark-to-beat, leading to more estimates of smaller values. However, this
474 affects only 12 % of the basins, as calibrated values between 0.2 and 0.5 are not frequently present in the calibration
475 result. Generally, the differences in KGE appear higher for smaller γ values, probably due to the decreasing pa-
476 rameter sensitivity with higher values (see Appendix B).

477 Given the variability in the performance of the regionalization methods across the depicted γ ranges, it is challeng-
478 ing to identify an overall best regionalization method using Fig. 4a. Therefore, we compare the various metrics of
479 the KGE values depicted in Fig. 4b. The analyzed metrics are the minimum, maximum, mean, and median. Further,
480 we count the number of poorly performing basins, defined as basins with a KGE below 0.2. In Fig. 4b, metrics
481 that exceed the benchmark-to-beat are grey-shaded. Comparing the KGE metrics in Fig. 4b reveals that the meth-
482 ods showing higher logMAE values in our split-sampling test ensemble also show lower performance in simulating
483 discharge. For example, all mean (and median) KGE values of the "worst" methods are below the mean KGE of
484 0.587 from the benchmark-to-beat, ranging from 0.545 to 0.578. This indicates that the used logMAE between
485 regionalized and calibrated values is a valid tool for a preliminary selection of adequate methods for the regional-
486 ization of WaterGAP3. However, for a more comprehensive analysis, we recommend additionally analyzing the
487 accuracy of simulated discharges, as the logMAE of calibrated and regionalized parameter values simplifies the
488 inherent complexity between model parameters and model performance.

489 Moreover, SI (best) outperforms the benchmark-to-beat in all listed metrics, reducing poorly performing basins
490 and enhancing well-performing basins. MLR (best) performs very similarly to SI (best), yet it shows a higher
491 number of basins with KGE values below 0.2. In comparison to the benchmark-to-beat, it outperforms four out of
492 five criteria. The remaining well-performing methods, SP and knn (best), demonstrate superior or equal perfor-
493 mance to the benchmark-to-beat in three out of five criteria. SP results in an equal number of poorly performing
494 basins, and the minimal KGE value is lower than for the benchmark-to-beat. The knn (best) approach has a slightly
495 worse median of KGE, i.e., -0.001, and one additional basin shows a KGE below 0.2.

496 As SI (best) outperforms the benchmark-to-beat in all metrics, we conduct a statistical test to ascertain whether
497 there is a statistically significant difference in KGE results between the methods. To this end, we use a one-sided
498 paired Wilcoxon rank sum test to test the null hypothesis of whether the KGE differs significantly in central ten-
499 dency. A significance level of 0.05 and an adjusted p-value are applied to correct for multiple comparisons (using
500 the correction after Benjamini & Hochberg (1995)). The results (cf. Figure F1c) demonstrate that SI (best) outper-
501 forms all "worst" methods and the benchmark-to-beat. However, the null hypothesis for SP and the "best" options

502 of knn and MLR cannot be rejected. Consequently, rather than identifying a single alternative to the benchmark-
503 to-beat, we have identified four.

504 Notably, all regionalization methods lead to poorly performing basins, as evidenced by the range of basins with a
505 KGE below 0.2, varying from 13 to 37. In Fig. 4c, we examine whether there are basins that all methods cannot
506 regionalize, thereby indicating a general insufficiency of the regionalization methods for these basins. The histo-
507 gram indicates that most poorly performing basins belong to a single regionalization method. The high number of
508 basins, which cannot be estimated well by a single regionalization method, illustrates the diverse shortcomings of
509 the methods. A single basin shows poor performance across all methods. This is a basin of the river El Platanito
510 in Mexico. The calibrated γ value is about 1.5, and the corresponding KGE value in calibration is 0.466. This basin
511 appears to be highly sensitive to γ , with an inaccuracy in the estimated γ having a significant impact on the accuracy
512 of river discharge. For example, the benchmark-to-beat estimates γ to 1.0, which is close to the calibrated value of
513 1.5. However, the KGE value of the simulated discharge using the benchmark-to-beat is -0.158 due to a high
514 overestimation of the variation and mean of the discharge. This high sensitivity seems outstanding and is likely
515 attributable to the absence of waterbodies and snow, supporting a potentially high impact of γ on the model simu-
516 lation (Kupzig et al., 2023) in conjunction with a relatively small basin size (ca. 6,600 km²).

517 Model evaluation is at least partially subjective (Ritter & Muñoz-Carpena, 2013), and the choice of evaluation
518 criteria represents a source of uncertainty in model performance evaluation (Onyutha, 2024). Furthermore, the
519 choice should reflect the intended model use (Janssen & Heuberger, 1995). As GHMs are often applied to evaluate
520 monthly simulated discharge (e.g., Herbert and Döll, 2023; Jones et al., 2023; Tilahun et al., 2024), we assess the
521 model performance using monthly data. Moreover, GHMs are generalists rather than expert models; thus, the
522 model evaluation should encompass a range of aspects related to streamflow to obtain an overall metric. Therefore,
523 we applied the monthly KGE, which comprises information about the streamflow's variability, bias, and timing.
524 As we use monthly values, we expect that outliers, i.e., single flood events, are less influential than in daily data
525 sets. Consequently, we expect the disadvantage of the KGE exhibiting sampling uncertainty to be less significant
526 (cf. Clark et al., 2021).

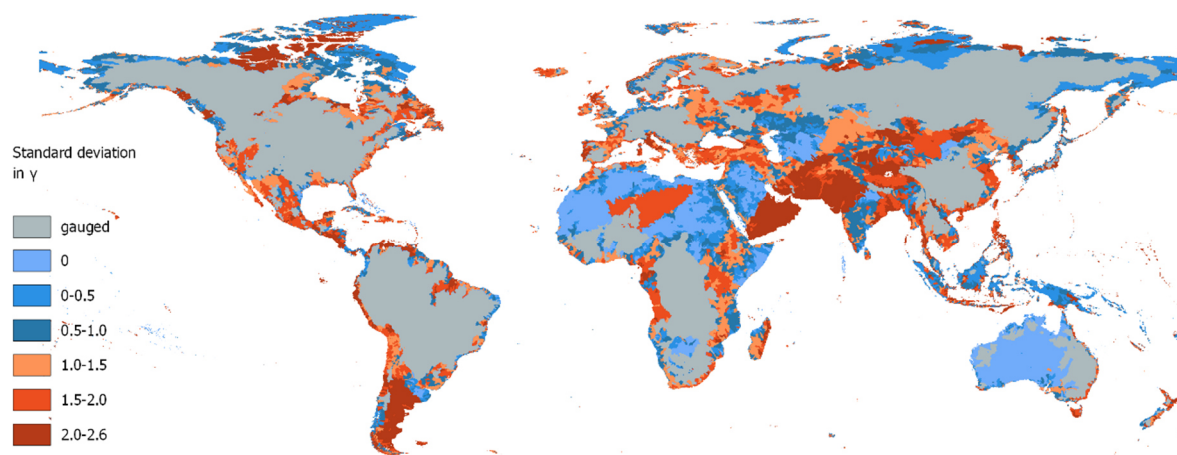
527 Nevertheless, to reduce the risk that disadvantages of the evaluation criteria influence the model evaluation, we
528 conducted an additional model evaluation using a modified version of the Nash-Sutcliffe efficiency (NSE) (Nash
529 & Sutcliffe, 1970). This modified NSE uses absolute differences instead of squared terms, leading to a metric that
530 is especially suitable as an overall measure (Krause et al., 2005). The results of the analysis are in Appendix F.
531 The high boxplot similarity between the modified NSE and the KGE confirms that the monthly KGE represents
532 the overall monthly model quality. Moreover, the statistical metrics of the modified NSE indicate that MLR (best),
533 in particular, outperforms the benchmark-to-beat. Applying the one-sided paired Wilcoxon rank sum test on the
534 modified NSE reveals that knn (best), SI (best), and the benchmark-to-beat deliver no statistically significant dif-
535 ferences in the central tendency to the well-performing MLR (best). These differences in results illustrate that the
536 choice of evaluation criteria can significantly impact the experimental outcome. Moreover, it underpins the use-
537 fulness of evaluating ensemble approaches to account for this inherent uncertainty.

538 **3.4 Impacts on runoff simulations**

539 To evaluate the impact of runoff simulations, we apply an ensemble of regionalization methods generating γ esti-
540 mates for the worldwide ungauged regions. Within the ensemble, we use the four methods SI (best), knn (best),

541 MLR (best), and SP that (1) outperform the benchmark-to-beat regarding the logMAE of regionalized and cali-
 542 brated values and (2) perform similarly to each other and better than the benchmark-to-beat in KGE for monthly
 543 discharge. Additionally, we use the benchmark-to-beat as the fifth member of our regionalization method ensemble,
 544 as it shows no significantly weaker performance than the well-performing MLR (best) for the modified NSE.
 545 The entire set of 933 gauged basins is used for regionalizing γ , resulting in five distinct worldwide distributions of
 546 γ . The spatially distributed standard deviation of the regionalized values is shown in Fig. 5.

547 In particular, the southern parts of South America, the northern and southern parts of North America, and Central
 548 Asia reveal differences in γ across the ensemble of regionalization methods (see Fig. 5). In Europe, the highest
 549 differences in regionalized values are observed in Italy, Great Britain, and northern Portugal. In Oceania, the high-
 550 est values in standard deviation of γ are in Tasmania, New Zealand, and the southwest of Australia's coast. In
 551 contrast, a minor variation in γ is apparent in northern Africa, most parts of Australia, and the East of the Dead
 552 Sea. Thus, the uncertainty associated with globally regionalizing γ seems to vary across different regions.



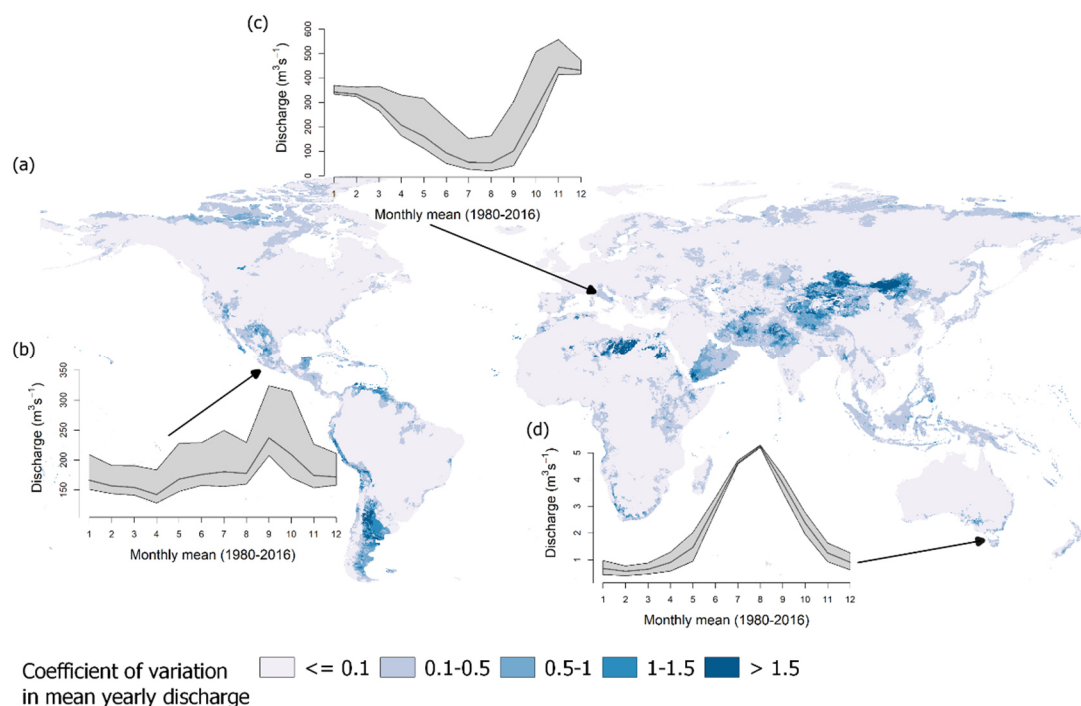
553 **Figure 5: Standard deviation in regionalized γ values using the best approaches of MLR (best), SI (best), SP, knn (best),**
 554 **and the benchmark-to-beat. Note that dry regions without discharge are set to zero.**
 555

556 An example of how these uncertainties in regionalized values propagate through the water system is presented in
 557 Fig. 6. This figure displays the coefficient of variation of the mean yearly discharge between 1980 and 2016 based
 558 on the five simulation runs. Moreover, we highlight the effect on rivers in ungauged regions by showing the re-
 559 sulting seasonal pattern, i.e., the simulated long-term mean of monthly river discharge for three exemplary rivers.
 560 These rivers are the Río Bravo in Mexico, the Tiber in Italy, and the Tamar River in Tasmania. Each river is located
 561 in an ungauged region, where the standard deviation in γ is high (see Fig. 5).

562 Comparing Fig. 5 and Fig. 6 reveals that regions showing variability in γ tend to exhibit variation in mean yearly
 563 discharge. However, the impact of variation in γ on the simulated discharge appears to vary spatially. Some regions
 564 showing a high degree of variation in γ do not exhibit a correspondingly high degree of variation in discharge. For
 565 example, 45 % of all ungauged regions showing a low variation in discharge, i.e., the coefficient of variation is
 566 below 0.5, exhibit a standard deviation of more than one in γ . In contrast, about 89 % of the ungauged regions
 567 showing a higher discharge variation exhibit a standard deviation of more than one in γ . Thus, variation in γ does
 568 not necessarily lead to variation in river discharge, but it increases the likelihood that a region's discharge is af-
 569 fected. The spatially varying impact of γ is likely related to varying sensitivity regarding γ in the ungauged regions,
 570 which depends on numerous aspects, e.g., snow occurrence or waterbodies (see Kupzig et al., 2023).

571 About 11 % of the ungauged area exhibits variations in yearly river discharge exceeding 50 % of the mean. These
 572 regions are primarily in southern South America and Central Asia. A further 62 % of the ungauged area exhibits
 573 variations in yearly river discharge between 10 % and 50 % of the mean. These regions are mainly located on the
 574 northern coast of Russia and northern Canada, Indonesia, and Tasmania. Other areas, like most ungauged regions
 575 of Africa and Australia, show almost no impact, i.e., the variation in yearly discharge is less than 10 % of the
 576 mean. In northern Africa, one region exhibits higher values in the coefficients of variation. These values are at-
 577 tributable to minimal discharge values, resulting in comparatively high coefficients of variation in this region.

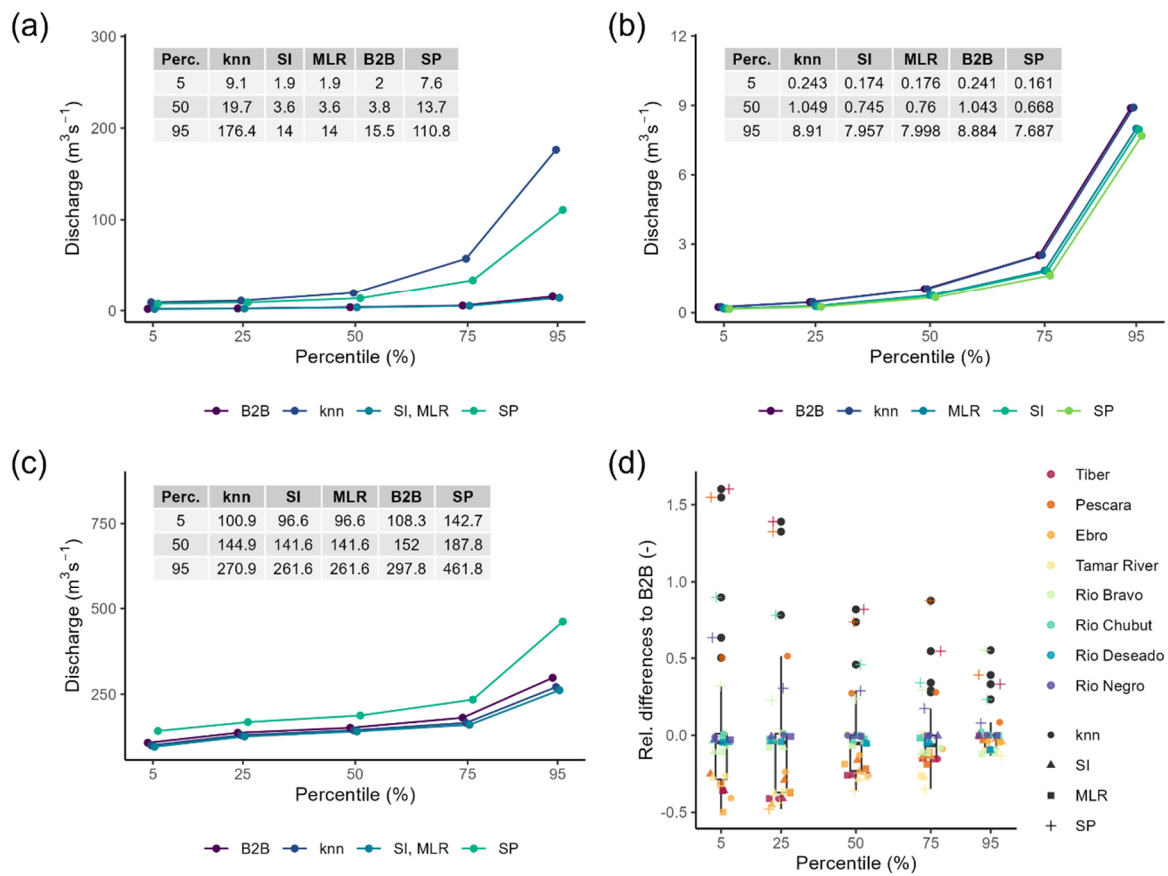
578 Considering the variation in the seasonality in the selected ungauged river systems (see Fig. 6b-d), the temporal
 579 impact of regionalization varies across the local landscape. For the Tamar River in Tasmania, as illustrated in Fig.
 580 6d, the variation is higher at the start and end of the dry periods in October/November and April/May, respectively.
 581 The spread in monthly mean discharge is about $0.7 \text{ m}^3\text{s}^{-1}$ to $1 \text{ m}^3\text{s}^{-1}$ in these periods. The Tiber in Italy and the Río
 582 Bravo in Mexico exhibit a similar pattern: using the regionalized γ values of SP leads to much higher discharge
 583 rates than other ensemble members, introducing broad uncertainty bands. For the Tiber, this leads to seasonal
 584 estimates varying between 1.2 % (in January) and 11 % (in October) of the mean yearly sum. The Río Bravo shows
 585 variations in its seasonal pattern, with values ranging from 2.2 % (in February) to 6.8 % (in October) of the mean
 586 yearly sum. Thus, all rivers display a temporally varying impact. Whereas the main variation in the discharge of
 587 the Río Bravo and the Tiber is mainly attributed to the SP regionalization run, for the Tamaris River, all regional-
 588 ization runs contribute to the varying long-term monthly mean in discharge.



590 **Figure 6: a) Global map of the coefficient of variation in mean yearly discharge for the applied regionalization methods.**
 591 **Resulting differences in the regionalization ensemble regarding the long-term mean of monthly discharge are depicted**
 592 **for: b) the Río Bravo in Mexico, c) the Tiber in Italy and d) the Tamar River in Tasmania. The grey-shaded area**
 593 **indicates the range of the long-term mean of monthly discharge and the black line indicates the mean off all simulation**
 594 **runs.**

595 To gain a deeper understanding of the local impact of regionalization on runoff simulations, we analyze the annual
 596 percentiles from 1980 to 2016 for Río Deseado in Argentina, Río Bravo, and Tamar River, displaying the mean
 597 percentile of all years (see Fig. 7a-c). As the Tiber and Río Bravo display high similarities in the resulting patterns

598 of percentiles, we demonstrate the impact by showing the percentiles from the Río Bravo. Additionally, we com-
 599 pare the relative differences in the mean for each percentile using eight ungauged river systems (see Fig. 7d), as
 600 previously done by Gudmundsson et al. (2012) for nine GHMs. To calculate the relative difference, we subtract
 601 the mean annual percentile of a method from the corresponding mean annual percentile of the reference and divide
 602 the resulting difference by the mean annual percentile of the reference. Instead of using observed flow as a refer-
 603 ence, we use the annual percentiles of our benchmark-to-beat. As river discharge is already spatially aggregated
 604 information, it is unnecessary to spatially aggregate grid cells to create results comparable to those of Gudmunds-
 605 son et al. (2012), who used cell runoff. The evaluated river systems are Río Chubut, Río Deseado, Río Negro, Río
 606 Bravo, Tamar River, Tiber, Pescara, and Ebro.



607

608 **Figure 7: Mean annual percentiles between 1980 and 2016 of simulated discharge using an ensemble of regionalization**
 609 **methods. The rivers are a) Río Deseado, b) Tamar River, and c) Río Bravo. In d), the relative differences in mean annual**
 610 **percentiles to the benchmark-to-beat of eight ungauged river systems are presented. Negative values indicate smaller**
 611 **mean annual percentiles than the benchmark-to-beat. Note that all data points from Río Deseado for knn and SP are**
 612 **excluded as the values are above 2.0.**

613 In Fig. 7a, Río Deseado is highly affected by uncertainties in simulated discharge due to the different regionaliza-
 614 tion methods; all segments of the percentiles show high variations where the absolute spread is increasing with
 615 increasing percentiles. For SP and knn (best), the discharge is highest, e.g., estimating a median discharge of 13.7
 616 m^3s^{-1} and 19.7 m^3s^{-1} , respectively. For the other methods, the simulated discharge is low, e.g., SI and MLR result
 617 in an equal median discharge of 3.6 m^3s^{-1} . The Tamar River in Fig. 7b also shows increasing absolute differences
 618 between the methods for higher percentiles, with the benchmark-to-beat approach leading to the highest discharge.
 619 For the Río Bravo, the absolute differences between the highest result of SP and the other methods remain almost
 620 constant until the 75th percentile. For the 95th percentile, the absolute differences increase rapidly from about 40

621 m^3s^{-1} (75th percentile) to nearly $200 \text{ m}^3\text{s}^{-1}$ (95th percentile). The exemplary results of Río Deseado and Río Bravo
 622 indicate a potentially high degree of uncertainty regarding the high percentiles in discharge simulation. These
 623 uncertainties put the results of global flood frequency analysis (e.g., Ward et al., 2013) in ungauged regions at risk
 624 as the time series of annual maxima might be even more uncertain. Thus, the results of flood frequency analysis
 625 should be carefully interpreted in ungauged regions as the impact of parameter regionalization may be significant.

626 Upon examination of the relative differences to the benchmark-to-beat for eight ungauged river systems, it be-
 627 comes evident that the impact of regionalization methods varies between ungauged river systems (e.g., Río Negro
 628 exhibits almost no variation, but Ebro does). Moreover, it becomes apparent that some regionalization methods
 629 contribute more to the variation in estimated discharge than others. The methods contributing most are knn (best)
 630 and SP. For knn (best), 10 of the 40 relative differences are higher than |0.3|. For SP, even 29 out of the 40 relative
 631 differences are higher than |0.3|. The results of SI (best) and MLR (best) are very similar, indicating high similarity
 632 in performance. This is consistent with the KGE evaluation (see Chapter 3.3), in which they performed similarly.
 633 The observation in Fig. 7d that higher relative differences of discharge simulations occur in drier percentiles is
 634 also reported in Gudmundsson et al. (2012). Moreover, the relative differences between the five regionalization
 635 runs seem comparable to the inter-model differences depicted in Gudmundsson et al. (2012), indicating the high
 636 impact of regionalization methods on the evaluated ungauged river systems.

637 Finally, Table 3 presents the estimated yearly mean runoff to the ocean for all five ensemble members. All esti-
 638 mates of global "runoff to ocean" range from 45,622 (SI (best)) to 47,069 (SP). Thus, the differences are on the
 639 scale of smaller inter-model differences (see Table 2 in Widen-Nilsson et al., 2007). The impact of regionalization
 640 becomes even more evident using an unsuitable regionalization method for WaterGAP3. For instance, the tuned
 641 kmeans ("subset") approach results in $42,862 \text{ km}^3 \text{ yr}^{-1}$ "runoff to ocean", increasing the spread between the meth-
 642 ods to $4,208 \text{ km}^3 \text{ yr}^{-1}$ being in the scale of inter-model differences. This high impact of regionalization on global
 643 "runoff to ocean" is surprising, given that only 27 % of the world is ungauged, using the GRDC database. From
 644 this 27 %, most regions are in Australia and Africa, where minimal runoff is produced. In studies employing
 645 disparate models, e.g., for inter-model comparison, all regions are simulated in disparate ways.

646 **Table 3: Mean outflow to the ocean and endorheic basins in $\text{km}^3 \text{ yr}^{-1}$ between 1980-2016. The highest continental devi-**
 647 **ation to the benchmark-to-beat is indicated in bold.**

<i>Runoff to ocean¹</i>	B2B	SI (best)	knn (best)	MLR (best)	SP
Oceania	1,127	-1.80 %	-2.20 %	-3.40 %	-6.60 %
Europe	3,098	-2.30 %	-0.10 %	-2.60 %	0.20%
Asia	16,676	3.50 %	0.30 %	1.60 %	5.50 %
Africa	5,203	-1.00 %	0.70 %	-0.30 %	-3.60 %
North America	7,517	0.30 %	1.00 %	-1.70 %	2.20 %
South America	12,032	1.30 %	1.40 %	-0.20 %	4.90 %
global	45,653	46,273	45,953	45,622	47,069

¹including endorheic basin

648 The most significant deviations in the continental sums of "runoff to ocean" in Table 3 are due to SP. Only for
 649 Europe is the highest deviation related to MLR (best), not SP. Interestingly, the estimated sums of SP occasionally
 650 define the lowest and occasionally the highest extremes for the continents, lacking a systematic pattern. The out-
 651 standing role of SP is consistent with previous evaluations in this Chapter, where SP frequently contributes most
 652 to the variation in discharge. This suggests that SP may not be suitable for the global scale. Nevertheless, the

653 pseudo-ungauged basins in the split-sample tests may also exhibit considerable distances from the observed basins.
654 Given that SP achieved satisfactory results in both evaluations, using either the logMAE or the KGE, the evaluation
655 indicates the method's suitability on a global scale. Thus, in the future, the split-sample test must be extended to
656 gain deeper insights into the method's robustness and make a definitive statement about the method's suitability
657 on a global scale. For example, the so-called "HDes" approach, recommended by Lebecherel et al. (2016), could
658 be applied for this purpose. In this approach, the closest basin to the corresponding (pseudo-) ungauged basin is
659 excluded from the regionalization process, thereby enabling an assessment of the method's robustness.

660 **3.5 Challenges & Future Directions**

661 Regionalization is an inevitable step when parameterizing GHMs. However, only a few studies exist that conduct
662 regionalization experiments with GHMs, often focusing on a single or two distinct regionalization strategies (e.g.,
663 Beck et al., 2016; Beck et al., 2020; Yoshida et al., 2022). A significant challenge in developing and testing dif-
664 ferent regionalization methods for GHMs is the time-consuming runtime of these models. This extensive runtime
665 impedes comprehensive testing of different regionalization methods, as evaluating the regionalization methods,
666 e.g., by using streamflow, demands a considerable number of simulation runs. This study addressed this challenge
667 using the differences between calibrated and regionalized parameter values as an approximator for the suitability
668 of the regionalization methods. Thereby, we considered the varying sensitivity of the parameter within the param-
669 eter space using the logMAE as the evaluation criterion. Using the differences between calibrated and estimated
670 values is the most straightforward approach, given that WaterGAP3 uses a single calibration parameter, leading to
671 a clear global optimum. However, this approach might not apply to GHMs using multiple calibration parameters
672 due to equifinality. For example, Ayzel et al. (2017) found varying estimated parameter values when regionalizing
673 11 parameters of the SWAP model using different regionalization methods. They concluded that the difference
674 between regionalized and calibrated values cannot be regarded as a performance measure due to parameter com-
675 pensation. Thus, further research is required to tackle the challenge of GHMs' time-consuming runtimes to enable
676 comprehensive testing of regionalization methods, especially for GHMs using multiple calibration parameters.

677 Another challenge in regionalizing hydrological models is the optimal selection of predictors for the regionaliza-
678 tion methods. Various approaches exist regarding the predictor selection for the regionalization methods (Razavi
679 & Coulibaly, 2013), resulting in a lack of consensus. This study used a predictor selection based on correlation
680 coefficients and an entropy assessment. The results indicate that the approach is particularly well-suited to the
681 Similarity Indices. However, further research on predictor selection is needed to find the optimal descriptor set
682 per method, as regionalization methods use predictors with varying efficiency. For example, future studies might
683 integrate feature importance bars, e.g., by using permutation, to identify the most critical descriptors per method.

684 Moreover, future research should explicitly account for the issue of multicollinearity. Multicollinearity can affect
685 MLR (and potentially other techniques), resulting in ungeneralizable predictions. This phenomenon is more
686 likely to occur when the number of predictor variables is large relative to the number of observation units and
687 when the predictor variables are highly collinear (Kiers & Smilde, 2007). To account for the high importance of
688 the generalizability of regionalization methods for GHMs, we used a high proportion of the basins for testing,
689 i.e., 50 %. Moreover, we used a large sample size (50 % of 933 basins) relative to the number of predictors
690 (maximum 12), lowering the risk of multicollinearity interfering with the results. However, future studies might
691 use methods such as Principal Component Analysis (PCA) or Partial Least Square (PLS), explicitly accounting

692 for the issue of multicollinearity (e.g., Kroll & Song, 2013). An alternative approach to using PCA or PLS is ex-
693 plicitly testing for multicollinearity in predictor sets using the variance inflation factor and avoiding using pre-
694 dictors with values exceeding a pre-defined threshold (e.g., Kroll et al., 2004).

695 **4. Conclusion**

696 Valid simulation results from GHMs, such as WaterGAP3, are crucial for detecting hotspots or studying patterns
697 in climate change impacts. However, the lack of worldwide monitoring data makes adapting GHMs' parameters
698 for valid global simulations challenging. Therefore, regionalization is necessary to estimate parameters in un-
699 gauged basins. This study applies regionalization methods for the first time to WaterGAP3, aiming to provide
700 insights into selecting suitable regionalization methods and evaluating their impact on the runoff simulations. Tra-
701 ditional and machine learning-based methods are tested to assess the application of several regionalization tech-
702 niques on a global scale. The concept of benchmark-to-beat and an ensemble of split-sampling tests are employed
703 for a comprehensive evaluation. Moreover, the impact on runoff simulation is assessed using a wide range of
704 temporal and spatial scales, i.e., from the daily to the yearly and from the local to the global scale.

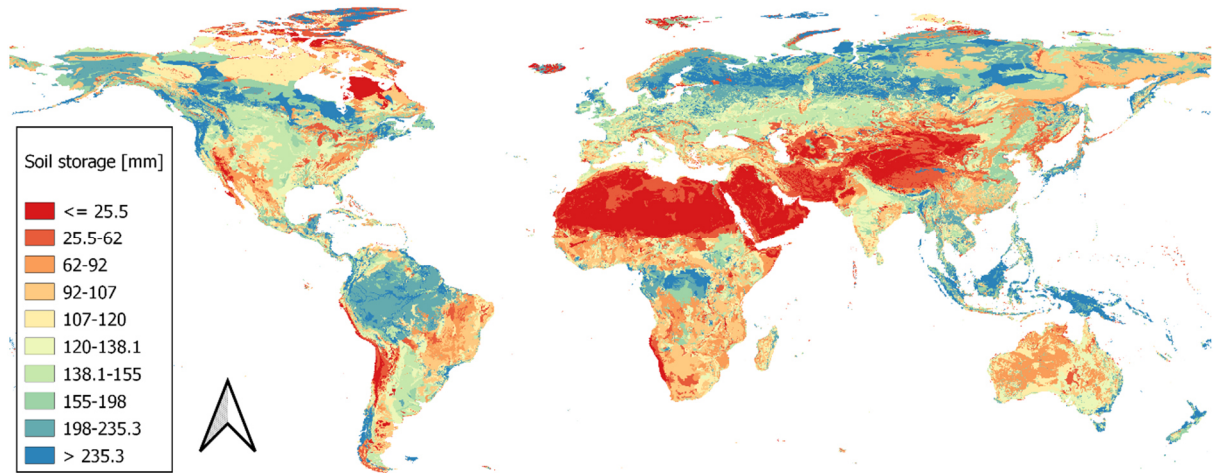
705 In this study, four regionalization methods outperform the benchmark-to-beat in monthly KGE and are thus con-
706 sidered appropriate for WaterGAP3. These methods span the complete range of methodologies, i.e., regression-
707 based methods and methods using the concept of physical similarity and spatial proximity. Moreover, the methods
708 vary in the descriptors used to achieve the highest accuracy. This highlights that different methods use descriptor
709 sets with varying efficiency. All methods perform best when using climatic and physiographic descriptors, indi-
710 cating that combining climatic and physiographic descriptors is optimal for regionalizing worldwide basins.
711 Mainly for two selected regionalization methods (tuned MLR and knn), the suggested descriptor selection based
712 on correlation coefficients and entropy assessment is not optimal. Further research might integrate variable im-
713 portance scores or PCA to enhance the predictor selection. Although random forest is known to be especially
714 robust among other machine learning-based techniques, it shows symptoms of over-parameterization, indicating
715 that the algorithm is too flexible and adjusts to noise in the data, missing the underlying systematic pattern.

716 Our results demonstrate that variation in the regionalized parameter value does not necessarily lead to variation in
717 river discharge. However, it increases the likelihood that a region's runoff is affected. This spatially varying impact
718 of γ is likely related to the varying sensitivity in ungauged regions regarding γ . Southern South America is a region
719 identified to be especially sensitive to variation in γ . Furthermore, local effects on runoff simulations indicate a
720 temporally varying impact. For example, some impacted rivers indicate a high degree of uncertainty regarding the
721 high percentiles in discharge simulation. These uncertainties potentially lead to a significant impact on flood fre-
722 quency analysis on a global scale, where the lack of gauging stations in certain regions calls for regionalization.
723 The global impact of regionalization methods that perform well for WaterGAP3 appears to be in the order of minor
724 inter-model differences. This impact rigorously increases when using a poorly performing method for WaterGAP3,
725 underscoring the importance of carefully selecting regionalization methods.

726 The spatial proximity approach contributes most to the variation in estimated runoff. The outstanding role of this
727 approach suggests that it may not be suitable for the global scale. However, as the pseudo-ungauged basins in the
728 split-sample tests may also have considerable large distances to the observed basins, and the method achieves
729 satisfactory results in all executed evaluations, it is not possible to make a definite statement about the method's

730 suitability for the global scale. Further research is required to gain deeper insights into the methods' robustness,
731 e.g., by extending the analysis by applying the recommended "HDes" approach (Lebecherel et al., 2016).

732 **Appendix A: Global Map of derived global soil moisture storage**



733
734 **Figure A1: Global map of the size of soil storage based on Batjes (2012) and land use information (derived from Friedl**
735 **& Sulla-Menashe, 2019)**

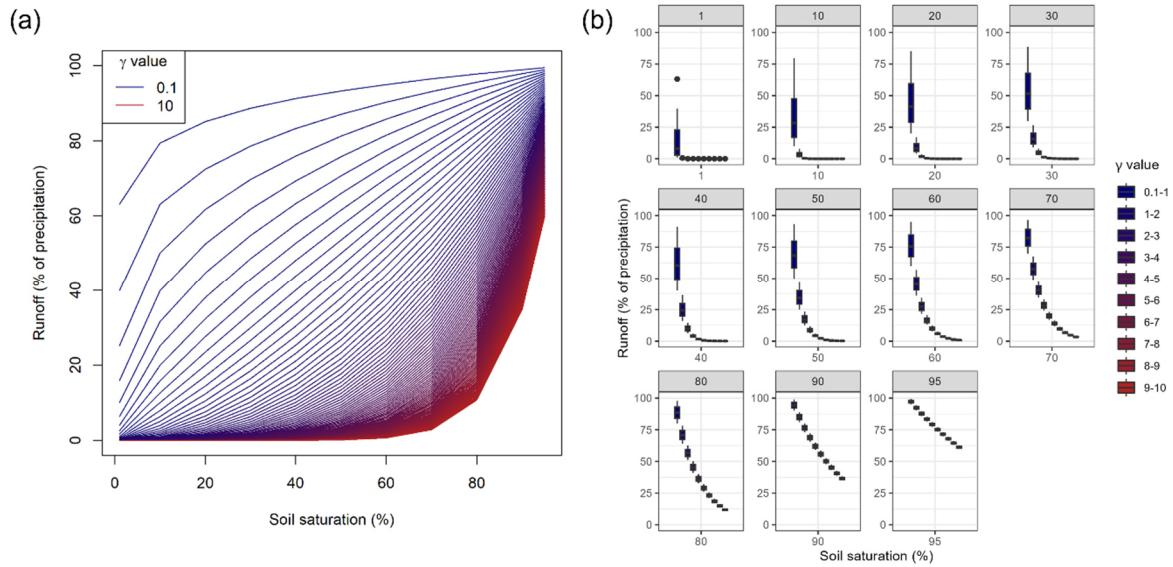
736 **Appendix B: Further analysis regarding the clustering of parameter values at the extremes**

737 The clustered calibrated parameter values at the extremes of the valid parameter space (see Fig. 1b) are a known
738 problem within the calibration. As the parameter space, i.e., the parameter bounds, is crucial for calibration and,
739 in consequence, for regionalization, we address this issue by a brief sensitivity analysis to demonstrate that the
740 clustering of the calibrated parameter values is more an issue of missing processes (or using additional parameter
741 values) than an issue of inappropriate parameter space. As the lower limit of the calibrated parameter (0.1) is
742 sufficiently small in comparison to other studies using a similar HBV-based approach for runoff generation pro-
743 cesses (e.g., see the beta in Table A2 in Jansen et al., 2022), we focus on the sensitivity analysis on the upper limit
744 of γ (5.0).

745 In the sensitivity analysis regarding the upper limit of γ , we applied the model formula (see equation B1) containing
746 the model's parameter γ and modified it within the bounds of 0.1 and 10. Additionally, we modified the soil satu-
747 ration varying from 1 % to 95 %.

$$outflow = precipitation_{effective} \cdot soil\ saturation^{\gamma} \quad (B1)$$

748 The calculated outflow and its relationship to the soil saturation and γ are depicted in Fig. B1 and B2. The incoming
749 effective precipitation is defined as constant. As it is a factor in equation B1, the results regarding incoming effec-
750 tive precipitation are linearly scalable.



751

752 **Figure B1: a) Runoff generation in the soil layer (neglecting overflow and evapotranspiration) using different values**
 753 **for the calibration parameter and increasing the soil-moisture, b) runoff generation for varying soil moisture grouped**
 754 **in bins of size one.**

755 In the depicted Fig. B1, the runoff generation process differences between differing γ values become more linear
 756 when soil saturation increases. Thus, the non-linear model parameter becomes less critical for high soil moisture.
 757 Generally, the runoff generation process differences for higher γ values are more pronounced for higher soil mois-
 758 ture. For lower soil moisture, the smaller values have higher effects on the generated runoff. For example, for 70 %
 759 soil moisture, the differences for γ values ranging from 5 to 10 are between 3 % and 16 %. For the same soil
 760 moisture, the range in runoff generation varies from 16 % to 70 % for γ values between 1 and 5.

761 High γ values usually occur in dry regions (see Fig. 4b in Müller Schmied et al., 2021). In dry regions, high soil
 762 moisture values are not expected to occur frequently (e.g., see Khosa et al., 2020; Oloruntoba et al., 2024 for
 763 estimated and measured soil moisture in Africa and Draper et al., 2008 for estimated and measured soil moisture
 764 in Australia). It is, therefore, unlikely that higher γ values will significantly enhance the calibration result or de-
 765 crease the issue of clustered calibrated parameter values at the higher end of the parameter space. More likely, the
 766 clustering of calibrated parameter values will be resolved in dry regions by incorporating additional (missing)
 767 model processes, such as evaporation from rivers or inaccurate representation of groundwater processes (Eisner,
 768 2016, p. 49). Thus, the parameter bounds of γ (e.g., also used in Eisner 2016, p. 16; Müller Schmied et al., 2021;
 769 Müller Schmied et al., 2023) are not changed in this study.

770 **Appendix C: Basin descriptors**

771 Overview of basins descriptors used in this study. All basin descriptors are derived from the original model input
 772 and aggregated with a simple mean method to basin values to produce the same spatial resolution as the calibrated
 773 model parameter.

- 774 • *Soil Storage*: The size of the soil storage, i.e., the maximal water content in the soil reachable for plants
 775 in mm. The information is the product of rooting depth (defined in a look-up table) and the total available
 776 water content derived from Batjes (2012).

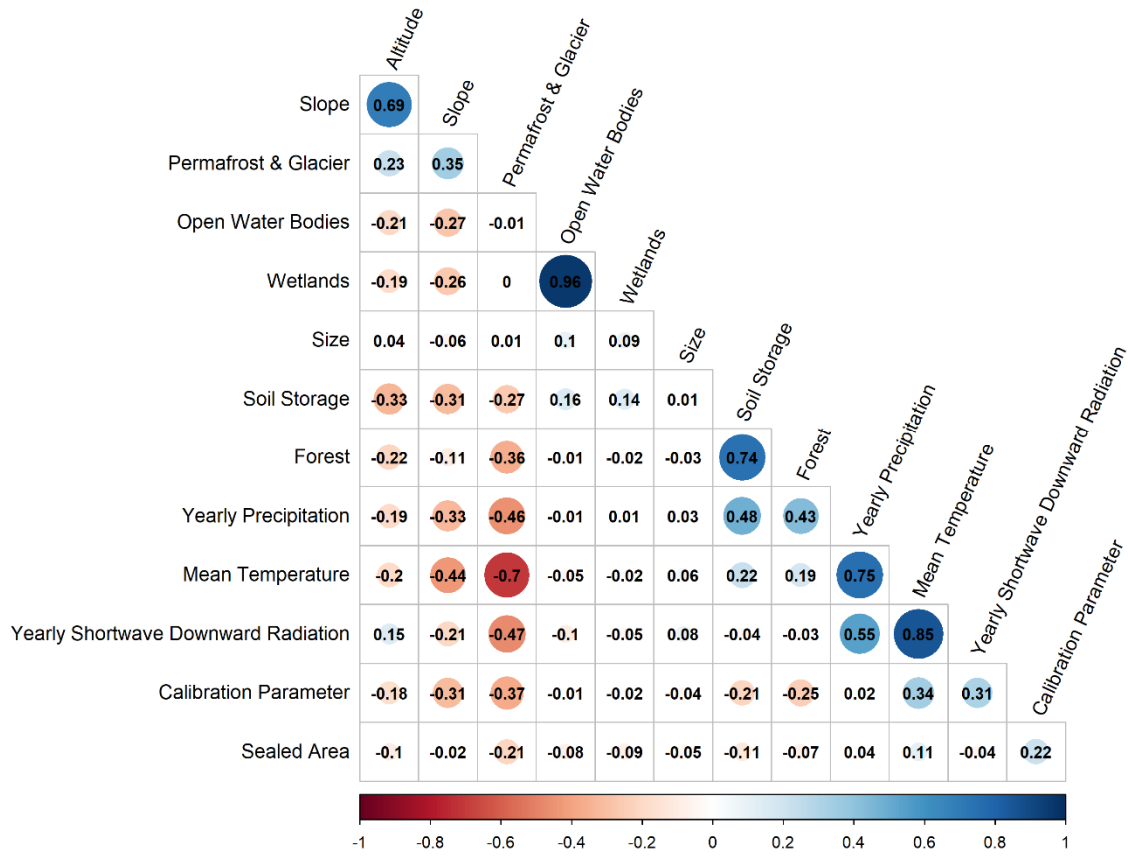
- 777 • *Open Water Bodies*: The fraction of the area covered with open water bodies in the basin is given as a
778 percentage. The model input is based on the GLWD database (Lehner & Döll, 2004).
- 779 • *Wetlands*: The fraction of area covered with wetlands in a basin is given in percentage. The model input
780 is based on the GLWD database (Lehner & Döll, 2004).
- 781 • *Size*: Size of a basin in km².
- 782 • *Slope*: The mean slope class is calculated as described in Döll & Fiedler (2008) and based on GTOPO30
783 (USGS EROS data centre).
- 784 • *Altitude*: The mean altitude of a basin is given in meters above sea level and based on GTOPO30 (USGS
785 EROS data centre).
- 786 • *Forest*: The mean fraction of the area covered with forest is given in percentage and derived from MODIS
787 data (Friedl & Sulla-Menashe, 2019), where 2001 is used as a reference. All grid cells having a dominant
788 International Geosphere-Biosphere Programme (IGBP) classification between one and five are defined
789 as "forest".
- 790 • *Sealed Area*: The mean fraction of sealed area is given in percentage and derived from MODIS data
791 (Friedl & Sulla-Menashe, 2019), where 2001 is used as a reference. All grid cells having an IGBP clas-
792 sification equal to 13 are defined as they would contain 60% of the sealed area. Note: The different treat-
793 ment of forest and sealed area is based on the required model input; whereas the land cover is a classified
794 value, the sealed area is a floating-point value.
- 795 • *Permafrost & Glacier*: The mean coverage of permafrost and glacier in a basin is given in percentage. It
796 is based on the World Glacier Inventory and the Circum-Arctic Map of Permafrost and Ground-Ice Con-
797 ditions.
- 798 • *Mean Temperature*: The mean air temperature is based on the meteorological forcing used to drive the
799 model (Lange, 2019) covering the period 1979 to 2016 and given in degrees Celsius.
- 800 • *Yearly Precipitation*: The yearly precipitation sum is based on the meteorological forcing used to drive
801 the model (Lange, 2019) covering the period 1979 to 2016 and given in mm.
- 802 • *Yearly Shortwave Downward Radiation*: The yearly shortwave downward radiation is based on the me-
803 teorological forcing used to drive the model (Lange, 2019) covering the period 1979 to 2016 and given
804 in Wm⁻².

805

806 The correlation between the defined basin descriptors is shown in Fig. A1. The variation within each basin de-
807 scriptor for basins used for regionalization is shown in Fig. A2.

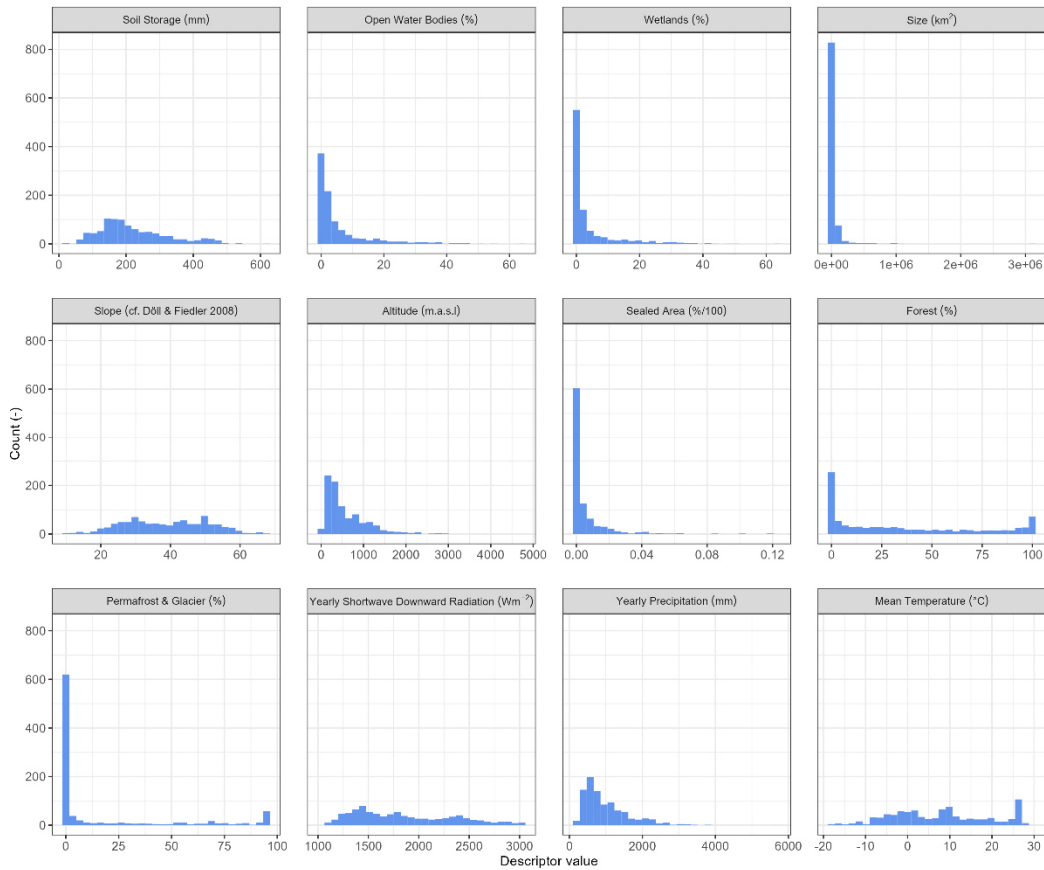
808

809



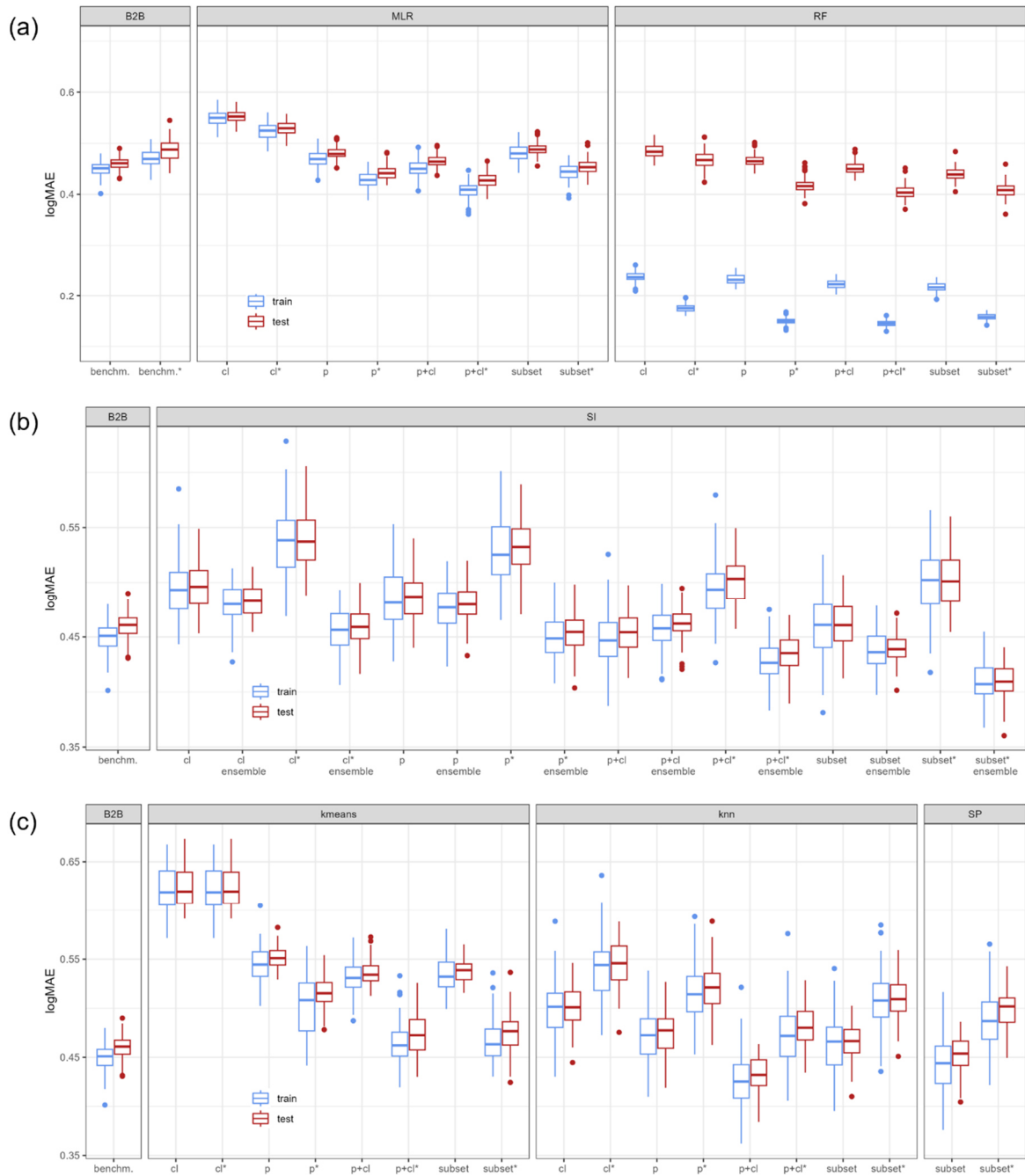
810
811
812

Figure C1: Correlation (using Pearson's correlation) between basins descriptors.



813
814

Figure C2: Distribution of basins descriptors within all basins used for regionalization (n=933)



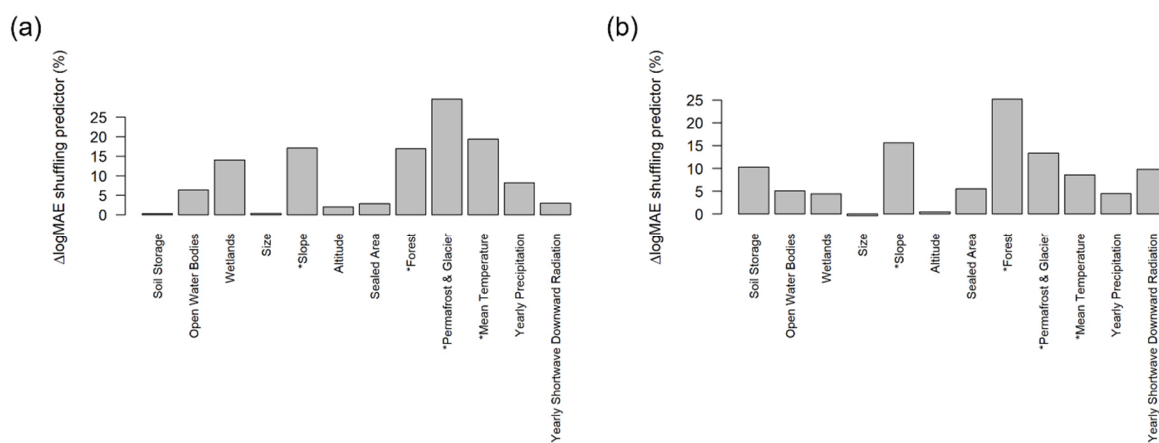
816
 817 **Figure D1: logMAE values for all 100 split-sampling tests using all variants of a) MLR, RF, and benchmark-to-beat,**
 818 **b) SI, and c) kmeans, knn, and SP. Note that the asterisk * indicates the tuned version of the method.**
 819

820 **Table D1: Performance loss in median logMAE of the ensemble of split-sample tests from training to testing expressed**
 821 **in % of logMAE in training.**

test (% train)	MLR	RF	SI		kmeans	knn	SP	B2B
			no ens.	ensem- ble				
cl	100.4	202.9	100.6	100.6	100	100	102.3	102.2
p	102.1	199.6	101.2	100.6	101.3	101.1		
p+cl	103.1	207.1	101.6	100.9	100.6	95.6		
subset	101.7	223.9	100	100.7	101.3	100.2		

test* (% train*)	MLR	RF	SI		kmeans	knn	SP	B2B
			no ens.	ensem- ble				
cl	100.8	266.9	99.8	100.7	100	100.4	103.1	104.1
p	103	277.3	101.3	101.3	101.4	101.4		
p+cl	104.4	277.9	102	102.1	102.2	101.7		
subset	102	258.2	99.8	100.5	103	100.2		

822 **Appendix E: Feature importance bars for MLR (best) and knn(best) using the descriptor set "p+cl"**



823
 824 **Figure E1: Decrease in logMAE for testing using one representative split-sample when randomly shuffling each pre-**
 825 **dictor for a) MLR (best) and b) knn (best). Note that the asterisk indicates the basin descriptors used in the (weakly)**
 826 **correlated subset.**

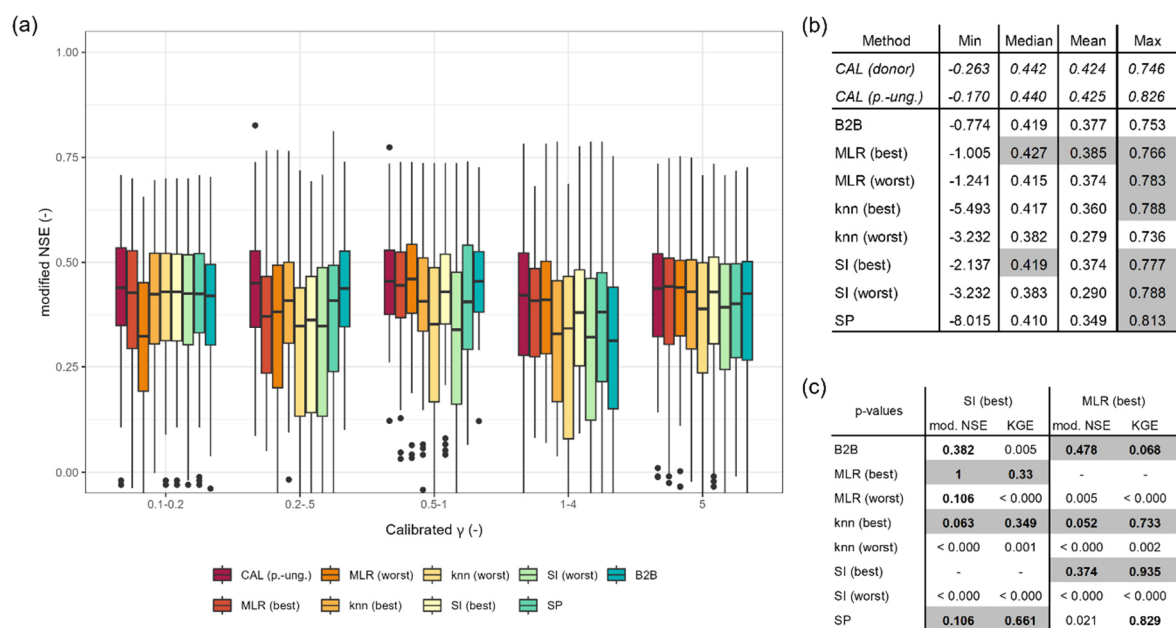
827 **Appendix F: Model performance for pseudo-ungauged basins using a modified version of the NSE**

828 Krause et al. (2005) suggested a modified version of the NSE that is especially suitable as an overall metric, leading
 829 to results between NSE versions focusing on low and high flows. The applied equation for the modified version is
 830 given below (see Eq. F1).

$$831 \text{ modified NSE} = 1 - \frac{\sum |y_k - x_k|}{\sum |y_k - \mu_y|} \quad (F1)$$

832 where x_k is the simulated monthly discharge for the timestep k and y_k is the observed discharge for the timestep
 833 k , and μ_y is the mean of the discharge for the evaluated period.

834 The evaluation of the modified NSE for all pseudo-ungauged basins of a representative split-sample are summa-
 835 rized in Figure F1. Note that the figure includes also the results of the applied one-sided paired Wilcoxon rank
 836 sum test for the KGE values, mentioned in Sect. 3.3.



837
 838 **Figure F1: a) modified NSE values of pseudo-ungauged basins from split-sample test grouped by the range**
 839 **of calibrated γ values, b) selected metrics of modified NSE values from the pseudo-ungauged basins (bet-**
 840 **ter or equal performance to the benchmark-to-beat is highlighted in grey), and c) p-values of the one-sided**
 841 **paired Wilcoxon rank sum test, testing the best performing methods MLR (best) and SI (best) against all**
 842 **other regionalization methods. (Note that p-values greater than 0.05 are highlighted in bold, indicating**
 843 **that the null hypothesis cannot be rejected, thus the difference in central tendency is not statistically sig-**
 844 **nificant; cases where the results of modified NSE and KGE indicate the same are shaded grey.)**

845
 846 *Code and data availability.* The data and the supporting R-Code to reproduce this study's findings are available at
 847 <https://doi.org/10.5281/zenodo.13122859>.

848 *Authors contribution.* JK developed, designed, and drafted the study. NK helped to design the experiment. MF
 849 provided feedback throughout the entire process and supported the writing.

850 *Competing interests.* The authors declare that they have no conflict of interest.

851
 852

853 **References**

- 854 Arheimer, B., Pimentel, R., Isberg, K., Crochemore, L., Andersson, J. C. M., Hasan, A., & Pineda, L.: Global
855 catchment modelling using World-Wide HYPE (WWH), open data, and stepwise parameter estimation, *Hydrology
856 and Earth System Sciences*, 24(2), 535–559. <https://doi.org/10.5194/hess-24-535-2020>, 2020.
- 857 Arsenault, R., & Brissette, F. P.: Continuous streamflow prediction in ungauged basins: The effects of equifinality
858 and parameter set selection on uncertainty in regionalization approaches, *Water Resources Research*, 50, 6135–
859 6153, <https://doi.org/10.1002/2013WR014898>, 2014.
- 860 Ayzel, G. V., Gusev, E. M., & Nasonova, O. N.: River runoff evaluation for ungauged watersheds by SWAP
861 model. 2. Application of methods of physiographic similarity and spatial geostatistics, *Water Resources*, 44(4),
862 547–558, <https://doi.org/10.1134/S0097807817040029>, 2017.
- 863 Barbarossa, V., Bosmans, J., Wanders, N., King, H., Bierkens, M. F. P., Huijbregts, M. A. J., & Schipper, A. M.:
864 Threats of global warming to the world's freshwater fishes, *Nature Communications*, 12(1), 1701,
865 <https://doi.org/10.1038/s41467-021-21655-w>, 2021.
- 866 Batjes, N. H.: ISRIC-WISE derived soil properties on a 5 by 5 arc-minutes global grid (ver. 1.2) [data set],
867 <https://data.isric.org/geonetwerk/srv/eng/catalog.search#/metadata/82f3d6b0-a045-4fe2-b960-6d05bc1f37c0>,
868 2012.
- 869 Beck, H. E., Pan, M., Lin, P., Seibert, J., van Dijk, A. I. J. M., & Wood, E. F.: Global Fully Distributed Parameter
870 Regionalization Based on Observed Streamflow From 4,229 Headwater Catchments, *Journal of Geophysical Re-
871 search: Atmospheres*, 125(17), <https://doi.org/10.1029/2019JD031485>, 2020.
- 872 Beck, H. E., van Dijk, A. I. J. M., Roo, A. de, Dutra, E., Fink, G., Orth, R. & Schellekens, J.: Global evaluation of
873 runoff from 10 state-of-the-art hydrological models, *Hydrol. Earth Syst. Sci.*, 21, 2881-20903,
874 <https://doi.org/10.5194/hess-21-2881-2017>, 2017.
- 875 Beck, H. E., van Dijk, A. I. J. M., Roo, A. de, Miralles, D. G., McVicar, T. R., Schellekens, J., & Bruijnzeel, L.
876 A.: Global-scale regionalization of hydrologic model parameters, *Water Resources Research*, 52(5), 3599–3622,
877 <https://doi.org/10.1002/2015WR018247>, 2016.
- 878 Benjamini, Y., & Hochberg, Y.: Controlling the False Discovery Rate: A Practical and Powerful Approach to
879 Multiple Testing, *Journal of the Royal Statistical Society. Series B (Methodological)*, 57(1), 289–300.
880 <http://www.jstor.org/stable/2346101>, 1995.
- 881 Boulange, J, Hanasaki, N, Yamazaki, D., & Pokhrel, Y.: Role of dams in reducing global flood exposure under
882 climate change, *Nature Communications*, 12(1), 417, <https://doi.org/10.1038/s41467-020-20704-0>, 2021.
- 883 Box, G. E. P., D. R. Cox: An analysis of transformations, *Journal of the Royal Statistical Society, Series B (Meth-
884 odological)*, 26 (2), 211 – 252, <https://www.jstor.org/stable/29844181964>, 1964.
- 885 Breimann, L.: Random Forests, *Machine Learning*, 45, 1–32, <https://doi.org/10.1023/A:1010933404324>, 2001.
- 886 Chaney, N. W., Herman, J. D., Ek, M. B., & Wood, E. F.: Deriving global parameter estimates for the Noah land
887 surface model using FLUXNET and machine learning, *Journal of Geophysical Research: Atmospheres*, 121(22),
888 13,218–13,235, <https://doi.org/10.1002/2016JD024821>, 2016.

889 Charrad, M., Ghazzali, N., Boiteau, V., Niknafs, A.: NbClust: An R Package for Determining the Relevant Number
890 of Clusters in a Data Set, *Journal of Statistical Software*, 61(6), 1–36. <https://doi.org/10.18637/jss.v061.i06>, 2014.

891 Clark, M. P., Vogel, R. M., Lamontagne, J. R., Mizukami, N., Knoben, W. J. M., Tang, G., Gharari, S., Freer, J.
892 E., Whitfield, P. H., Shook, K., Papalexiou, S. M.: The abuse of popular performance metrics in hydrologic mod-
893 elling, *Water Resources Research*, 57, e2020WR029001, <https://doi.org/10.1029/2020WR029001>, 2021. Cuntz,
894 M., Mai, J., Samaniego, L., Clark, M., Wulfmeyer, V., Branch, O., Attinger, S., & Thober, S.: The impact of stand-
895 ard and hard-coded parameters on the hydrologic fluxes in the Noah-MP land surface model, *Journal of Geophys-
896 ical Research: Atmospheres*, 121, 10,676 - 10,700, <https://doi.org/10.1002/2016JD025097>, 2016.

897 Döll, P. & Fiedler, K.: Global-scale modeling of groundwater recharge, *Hydrol. Earth Syst. Sci.*, 12, 863–885,
898 <https://doi.org/10.5194/hess-12-863-2008>, 2008

899 Döll, P., Kaspar, F., & Lehner, B.: A global hydrological model for deriving water availability indicators: model
900 tuning and validation, *Journal of Hydrology*, 270, 105–13, [https://doi.org/10.1016/S0022-1694\(02\)00283-4](https://doi.org/10.1016/S0022-1694(02)00283-4), 2003.

901 Döll, P., Hasan, H. M. M., Schulze, K., Gerdener, H., Börger, L., Shadkam, S., Ackermann, S., Hosseini-Moghari,
902 S.-M., Müller Schmied, H., Güntner, A., & Kusche, J.: Averaging multi-variable observations to reduce and quan-
903 tify the output uncertainty of a global hydrological model: evaluation of three ensemble-based approaches for the
904 Mississippi River basin, *Hydrology and Earth System Sciences*, 28 (10), 2259-2295, <https://doi.org/10.5194/hess-28-2259-2024>, 2024.

906 Draper, C. S., Walker, J. P., Steinle, P. J., de Jeu, R. A. M., Holmes T. R. H.: An evaluation of AMSR–E derived
907 soil moisture over Australia, *Remote Sensing of Environment*, 113, 703-710,
908 <https://doi.org/10.1016/j.rse.2008.11.011>, 2008.

909 Eisner, S.: Comprehensive Evaluation of the WaterGAP3 Model across Climatic, Physiographic, and Anthropo-
910 genic Gradients, Ph.D. thesis, University of Kassel, Kassel, Germany, 128pp., 2016.

911 Friedl, M., Sulla-Menashe, D.: MCD12Q1 MODIS/Terra+Aqua Land, Cover Type Yearly L3 Global 500m SIN
912 Grid V006, NASA EOSDIS Land Processes DAAC [data set], <https://doi.org/10.5067/MODIS/MCD12Q1.006>,
913 2019.

914 Feigl, M., Thober, S., Schweppe, R., Herrnegger, M., Samaniego, L., & Schulz, K.: Automatic Regionalization of
915 Model Parameters for Hydrological Models, *Water Resources Research*, 58, e2022WR031966,
916 <https://doi.org/10.1029/2022WR031966>, 2022.

917 Flörke, M., Kynast, E., Eisner, S., Verzano, K., Kupzig, J., Voß, F., Lehner, B., Rivera, J., aus der Beek, T., aus
918 der Beek, M., Malsy, M., & Alcamo, J.: WaterGAP3 (v1.0.0), Zenodo [software], [https://doi.org/10.5281/ze-
919 nodo.10940380](https://doi.org/10.5281/zenodo.10940380), 2024.

920 Golian, S., Murphy, C., & Meresa, H.: Regionalization of hydrological models for flow estimation in ungauged
921 catchments in Ireland, *Journal of Hydrology: Regional Studies*, 36, 100859,
922 <https://doi.org/10.1016/j.ejrh.2021.100859>, 2021.

923 GRDC, The Global Runoff Data Centre, 56068 Koblenz, Germany, 2020.

924 Gudmundsson, L., Tallaksen, L. M., Stahl, K., Clark, D. B., Dumont, E., Hagemann, S., Bertrand, N., Gerten, D.,
925 Heinke, J., Hanasaki, N., Voss, F., & Koirala, S.: Comparing Large-Scale Hydrological Model Simulations to

926 Observed Runoff Percentiles in Europe. *Journal of Hydrometeorology*, 13(2), 604-620.
927 <https://doi.org/10.1175/JHM-D-11-083.1>, 2012.

928 Guo Y, Zhang Y, Zhang L, & Wang Z: Regionalization of hydrological modeling for predicting streamflow in
929 ungauged catchments: A comprehensive review, *WIREs Water*, 8, e1487, <https://doi.org/10.1002/wat2.1487>,
930 2020.

931 Gupta, H. V., Kling, H., Yilmaz, K.K., Martinez, G. F.: Decomposition of the mean squared error and NSE per-
932 formance criteria: Implications for improving hydrological modelling, *Journal of Hydrology*, 377, 80-91,
933 <https://doi.org/10.1016/j.jhydrol.2009.08.003>, 2009.

934 Gupta, H. V, Sorooshian, S., & Yapo, P. O.: Toward improved calibration of hydrologic models: Multiple and
935 noncommensurable measures of information, *Water Resources Research*, 34(4), 751-763,
936 <https://doi.org/10.1029/97WR03495>, 1998.

937 He, Y., Bárdossy, A., & Zehe, E.: A review of regionalisation for continuous streamflow simulation, *Hydrology
938 and Earth System Sciences*, 15(11), 3539-3553. <https://doi.org/10.5194/hess-15-3539-2011>, 2011.

939 Herbert, C., Döll, P.: Analyzing the informative value of alternative hazard indicators for monitoring drought
940 hazard for human water supply and river ecosystems at the global scale, *Natural Hazards and Earth System Sci-
941 ences*, 23, 2111-2131, <https://doi.org/10.5194/nhess-23-2111-2023>, 2023.

942 Jansen, K. F., Teuling, A. J., Craig, J. R., Dal Molin, M., Knoben, W. J. M., Parajka, J., Vis, M., Melsen, L. A.:
943 Mimicry of a conceptual hydrological model (HBV): What's in a name? *Water Resources Research*, 57,
944 e2020WR029143. <https://doi.org/10.1029/2020WR029143>, 2022.

945 Janssen, P. H. M., Heuberger, P.S.C.: Calibration of process-oriented models, *Ecological Modelling*, 83 (1-2), 55-
946 66, [https://doi.org/10.1016/0304-3800\(95\)00084-9](https://doi.org/10.1016/0304-3800(95)00084-9), 1995.

947 Jones, E. R., Bierkens, M. F. P., van Vliet, M. T. H.: Current and future global water scarcity intensifies when
948 accounting for surface water quality, *Nature Climate Change*, 14, 629-635, [https://doi.org/10.1038/s41558-024-
949 02007-0](https://doi.org/10.1038/s41558-024-

949 02007-0), 2024.

950 Kaspar, F.: Entwicklung und Unsicherheitsanalyse eines globalen hydrologischen Modells, Ph.D. thesis, Univer-
951 sity of Kassel, Kassel, Germany, 129pp., 2004.

952 Khosa, F. V., Mateyisi, M. J., van der Merwe, M. R., Feig, G. T., Engelbrecht, F. A., Savage, M. J.: Evaluation of
953 soil moisture from CCAM-CABLE simulation, satellite-based models estimates and satellite observations: a case
954 study of Skukuza and Malopeni flux towers, *Hydrology and Earth System Sciences*, 24(4), 1587-1609,
955 <https://doi.org/10.5194/hess-24-1587-2020>, 2020.

956 Kiers, H.A.L., Smilde, A.K: A comparison of various methods for multivariate regression with highly collinear
957 variables, *Stat. Meth. & Appl.*, 16, 193-228, <https://doi.org/10.1007/s10260-006-0025-5>, 2007.

958 Krabbenhoft, C. A., Allen, G. H., Lin, P., Godsey, S. E., Allen, D. C., Burrows, R. M., DelVecchia, A. G., Fritz,
959 K. M., Shanafield, M., Burgin, A. J., Zimmer, M. A., Datry, T., Dodds, W. K., Jones, C. N., Mims, M. C., Franklin,
960 C., Hammond, J. C., Zipper, S., Ward, A. S., Olden, J. D.: Assessing placement bias of the global river gauge
961 network, *Nature Sustainability*, 5, 586-592. <https://doi.org/10.1038/s41893-022-00873-0>, 2022.

962 Krause, P. Boyle, D. P., Bäse, F.: Comparison of different efficiency criteria for hydrological model assessment,
963 *Advances in Geosciences*, 5, 89-97, <https://doi.org/10.5194/adgeo-5-89-2005>, 2005.

964 Kroll C., Lutz, J., Allen, B., Vogel, R.M.: Developing a Watershed Characteristics Database to Improve Low
965 Streamflow Prediction, *Journal of Hydrologic Engineering*, 9 (2), 116-125, [https://doi.org/10.1061/\(ASCE\)1084-0699\(2004\)9:2\(116\)](https://doi.org/10.1061/(ASCE)1084-0699(2004)9:2(116)), 2004.

967 Kroll, C. N., Song P.: Impact of Multicollinearity on Small Sample Hydrologic Regression Models, *Water Re-*
968 *sources Research*, 49, 3756-3769, <https://doi.org/10.1002/wrcr.20315>, 2013.

969 Kupzig, J., Reinecke, R., Pianosi, F., Flörke, M., & Wagener, T.: Towards parameter estimation in global hydro-
970 logical models, *Environmental Research Letters*, 18(7), 74023. <https://doi.org/10.1088/1748-9326/acdae8>, 2023.

971 Lange, S.: Earth2Observe, WFDEI and ERA-Interim data Merged and Bias-corrected for ISIMIP (EWEMBI), V.
972 1.1, GFZ Data Services [data set], <https://doi.org/10.5880/pik.2019.004>, 2019.

973 Lebecherel, L., Andréassian, V., Perrin: On evaluating the robustness of spatial-proximity-based regionalization
974 methods, *Journal of Hydrology*, 539, 196-203, <https://doi.org/10.1016/j.jhydrol.2016.05.031>, 2016.

975 Lehner, B. and Döll, P.: Development and validation of a global database of lakes, reservoirs and wetlands, *Journal*
976 *of Hydrology*, 296 (1-4), 1-22, <https://doi.org/10.1016/j.jhydrol.2004.03.028>, 2004.

977 Lehner, B., Verdin, K., & Jarvis, A.: New global hydrography derived from spaceborne elevation data, *Eos, Trans-*
978 *actions, AGU*, 89, 93–94, doi:10.1029/2008EO100001, 2008.

979 Liam, A., & Wiener, M.: Classification and Regression by randomForest. *R News*, 2(3), 18–22, 2002.

980 Lindström, G., Johansson, B., Persson, M., Gardelin, M., & Bergström, S.: Development and test of the distributed
981 HBV-96 hydrological model, *Journal of Hydrology*, 201, 272–288, [https://doi.org/10.1016/S0022-1694\(97\)00041-3](https://doi.org/10.1016/S0022-1694(97)00041-3), 1997.

983 McIntyre, N, Lee, H., Wheeler, H., Young, A., & Wagener, T.: Ensemble predictions of runoff in ungauged catch-
984 ments, *Water Resources Research*, 41(12), W12434, <https://doi.org/10.1029/2005WR004289>, 2005.

985 Merz, R., Blöschl, G.: Regionalisation of catchment model parameters, *Journal of Hydrology*, 287, 95-123,
986 <https://doi.org/10.1016/j.jhydrol.2003.09.028>, 2004.

987 Müller Schmied, H., Cáceres, D., Eisner, S., Flörke, M., Herbert, C., Niemann, C., Peiris, T. A., Popat, E., Port-
988 mann, F. T., Reinecke, R., Schumacher, M., Shadkam, S., Telteu, C.-E., Trautmann, T., Döll, P.: The global water
989 resources and use model WaterGAP v2.2d: model description and evaluation, *Geoscientific Model Development*,
990 14(2), 1037–1079, <https://doi.org/10.5194/gmd-14-1037-2021>, 2021.

991 Müller Schmied, H., Trautmann, T., Ackermann, S., Cáceres, D., Flörke, M., Gerdener, H., Kynast, E., Peiris, T.
992 A., Schiebener, L., Schumacher, M., Döll, P.: The global water resources and use model WaterGAP v2.2e: de-
993 scription and evaluation of modifications and new features, *Geoscientific Model Development Discussions* [pre-
994 print], 1-46, <https://doi.org/10.5194/gmd-2023-213>, 2023.

995 Nash, J. E., Sutcliffe, J. V.: River flow forecasting through conceptual models part I — A discussion of principles,
996 *Journal of Hydrology*, 10 (3), 282-290, [https://doi.org/10.1016/0022-1694\(70\)90255-6](https://doi.org/10.1016/0022-1694(70)90255-6), 1970.

- 997 Nijssen, B., O'Donnell, G. M., Lettenmeier, D. P., Lohmann, D., & Wood, E. F.: Predicting the Discharge of
998 Global Rivers, American Meteorological Society, 3307–3323, [https://doi.org/10.1175/1520-0442\(2001\)014<3307:PTDOGR>2.0.CO;2](https://doi.org/10.1175/1520-0442(2001)014<3307:PTDOGR>2.0.CO;2), 2000.
- 1000 Oloruntoba, B., Kollet, S., Motzka, C., Vereecken H., Franssen H.-J. H.: High Resolution Land Surface Modelling
1001 over Africa: the role of uncertain soil properties in combination with temporal model resolution, EGU sphere Pre-
1002 print repository [preprint], <https://doi.org/10.5194/egusphere-2023-3132>, 2024.
- 1003 Onyutha, C: Pros and cons of various efficiency criteria for hydrological model performance evaluation, Proceed-
1004 ings of IAHS, 385, 181–187, <https://piahs.copernicus.org/articles/385/181/2024/>, 2024.
- 1005 Oudin, L., Andréassian, V., Perrin, C., Michel, C., & Le Moine, N.: Spatial proximity, physical similarity, regres-
1006 sion and ungauged catchments: A comparison of regionalization approaches based on 913 French catchments, Wa-
1007 ter Resources Research, 44(3), W03413, <https://doi.org/10.1029/2007WR006240>, 2008.
- 1008 Oudin, L., Kay, A., Andréassian, V., & Perrin, C.: Are seemingly physically similar catchments truly hydrologi-
1009 cally similar? Water Resources Research, 46(11), W11558, <https://doi.org/10.1029/2009WR008887>, 2010.
- 1010 Pagliero, L., Bouraoui, F., Diels, J., Willems, P., & McIntyre, N.: Investigating regionalization techniques for
1011 large-scale hydrological modelling, Journal of Hydrology, 570, 220–235, <https://doi.org/10.1016/j.jhydrol.2018.12.071>, 2019.
- 1013 Parajka, J., Merz, R., & Blöschl, G.: A comparison of regionalisation methods for catchment model parameters,
1014 Hydrology and Earth System Sciences, 9, 157–171, <https://doi.org/10.5194/hess-9-157-2005>, 2005.
- 1015 Poissant, D., Arsenault, R. & Brissette, F.: Impact of parameter set dimensionality and calibration procedures on
1016 streamflow prediction at ungauged catchments, Journal of Hydrology: Regional Studies, 12, 220–237,
1017 <https://doi.org/10.1016/j.ejrh.2017.05.005>, 2017.
- 1018 Pool, S., Vis, M., & Seibert, J.: Regionalization for ungauged catchments — Lessons learned from a comparative
1019 large-sample study. Water Resources Research, 57, e2021WR030437. <https://doi.org/10.1029/2021WR030437>,
1020 2021.
- 1021 Qi, W., Chen, J., Li, L., Xu, C., Li, J., Xiang, Y., & Zhang, S.: A framework to regionalize conceptual model
1022 parameters for global hydrological modelling, Hydrology and Earth System Sciences Discussions [preprint],
1023 <https://doi.org/10.5194/hess-2020-127>, 2020.
- 1024 R Core Team.: R: A language and environment for statistical computing R Foundation for Statistical Computing,
1025 Vienna, Austria. <https://www.r-project.org/>, 2020.
- 1026 Razavi, T., Coulibaly, P.: Streamflow Prediction in Ungauged Basins: Review of Regionalization Methods, Jour-
1027 nal of Hydrologic Engineering, 18 (8), 958–975, <https://ascelibrary.org/doi/abs/10.1061/%28ASCE%29HE.1943-5584.0000690>, 2013.
- 1029 Reichl, J. P. C., Western, A. W., McIntyre, N. R. & Chiew, F. H. S: Optimization of a Similarity Measure for
1030 Estimating Ungauged Streamflow, Water Resources Research, 45 (10), <https://doi.org/10.1029/2008WR007248>,
1031 2009.

- 1032 Ritter, A., Muñoz-Carpena R.: Performance evaluation of hydrological models: Statistical significance for reducing
1033 subjectivity in goodness-of-fit assessments, *Journal of Hydrology*, 480, 33-45, <https://doi.org/10.1016/j.jhydrol.2012.12.004>, 2013. Samaniego, L, Kumar, R & Attinger, S.: Multiscale parameter regionalization of a grid-
1034 based hydrologic model at the mesoscale, *Water Resources Research*, 46(5), W05523,
1035 <https://doi.org/10.1029/2008WR007327>, 2010.
- 1037 Schaefli, B., & Gupta, H. V.: Do Nash values have value?, *Hydrological Processes*, 21(15), 2075–2080,
1038 <https://doi.org/10.1002/hyp.6825>, 2007.
- 1039 Schweppe, R., Thober, S., Müller, S., Kelbling, M., Kumar, R., Attinger, S., & Samaniego, L.: MPR 1.0: a stand-
1040 alone multiscale parameter regionalization tool for improved parameter estimation of land surface models, *Geo-
1041 scientific Model Development*, 15, 859–882, <https://doi.org/10.5194/gmd-15-859-2022>, 2022.
- 1042 Seibert, J.: On the need for benchmarks in hydrological modelling, *Hydrological Processes*, 15(6), 1063–1064,
1043 <https://doi.org/10.1002/hyp.446>, 2001.
- 1044 Seibert, J., Staudinger, M., van Meerveld, H. J. I: Validation and Over-Parameterization – Experiences from Hy-
1045 drological Modeling, in: *Computer Simulation Validation*, edited by: Breisbart, C. Saam, J. S., Springer Nature
1046 Switzerland, Cham, Switzerland, 811-834, <https://doi.org/10.1007/978-3-319-70766-2>, 2019.
- 1047 Shannon, C. E.: A Mathematical Theory of Communication, *The Bell System Technical Journal*, 3(27), 379-423,
1048 <https://doi.org/10.1002/j.1538-7305.1948.tb01338.x>, 1948.
- 1049 Stacke, T., & Hagemann, S.: HydroPy (v1.0): a new global hydrological model written in Python, *Geoscientific
1050 Model Development*, 14, 7795–7816, <https://doi.org/10.5194/gmd-14-7795-2021>, 2021.
- 1051 Tang, Y., Marshall, L., Sharma, A. & Smith, T.: Tools for investigating the prior distribution in Bayesian hydro-
1052 logy, *Journal of Hydrology*, 538, 551-562, <https://doi.org/10.1016/j.jhydrol.2016.04.032>, 2016.
- 1053 Tilahun, A. B., Dürr, H. H., Schweden, K., Flörke, M.: Perspectives on total phosphorus response in rivers: Ex-
1054 amining the influence of rainfall extremes and post-dry rainfall, *Science of the Total Environment*, 940, 173677,
1055 <https://doi.org/10.1016/j.scitotenv.2024.173677>, 2024.
- 1056 Tongal, H., & Sivakumar, B.: Cross-entropy clustering framework for catchment classification, *Journal of Hydrol-
1057 ogy*, 552, 433–446, <https://doi.org/10.1016/j.jhydrol.2017.07.005>, 2017.
- 1058 Venables, W. N., & Ripley, B. D.: *Modern Applied Statistics with S (Fourth Edition)*. Springer Science+Business
1059 Media New York, USA, 501pp, ISBN 978-1-4419-3008-8, 2002
- 1060 Wagener, T., Wheeler, H. S., & Gupta, H. V.: *Rainfall – Runoff Modelling in Gauged and Ungauged Catchments*,
1061 Imperial College Press, London, UK, 332pp., <https://doi.org/10.1142/p335>, 2004.
- 1062 Wagener, T., & Wheeler, H. S.: Parameter estimation and regionalization for continuous rainfall-runoff models
1063 including uncertainty, *Journal of Hydrology*, 320, 132-154, <https://doi.org/10.1016/j.jhydrol.2005.07.015>, 2006.
- 1064 Ward, P. J., Jongman, B., Sperna Weiland, F., Bouwman, A., Van Beek, R., Bierkens, M. F. P., Ligtoet, W., &
1065 Winsemius, H. C.: Assessing flood risk at the global scale: model setup, results, and sensitivity, *Environmental
1066 Research Letters*, 8, Article 044019. <https://doi.org/10.1088/1748-9326/8/4/044019>, 2013 Widén-Nilsson, E.,
1067 Halldin, S., & Xu, C.: Global water-balance modelling with WASMOD-M: Parameter estimation and regionalisa-
1068 tion, *Journal of Hydrology*, 340(1-2), 105–118, <https://doi.org/10.1016/j.jhydrol.2007.04.002>, 2007.

- 1069 Wu, H., Zhang, J., Bao, Z., Wang, G., Wang, W., Yang, Y. & Wang, J.: Runoff Modeling in Ungauged Catchments
1070 Using Machine Learning Algorithm-Based Model Parameters Regionalization Methodology, *Engineering*, 28, 93-
1071 104, <https://doi.org/10.1016/j.eng.2021.12.014>, 2023.
- 1072 Yang, X., Magnusson, J., Huang, S., Beldring, S., & Xu, C.: Dependence of regionalization methods on the com-
1073 plexity of hydrological models in multiple climatic regions, *Journal of Hydrology*, 582, 124357,
1074 <https://doi.org/10.1016/j.jhydrol.2019.124357>, 2020.
- 1075 Yoshida, T., Hanasaki, N, Nishina, K., Boulange, J, Okada, M., & Troch, P. A.: Inference of Parameters for a
1076 Global Hydrological Model: Identifiability and Predictive Uncertainties of Climate-Based Parameters, *Water Re-
1077 sources Research*, 58, e2021WR03066, <https://doi.org/10.1029/2021WR030660>, 2022.